Design and Application of Low Compaction Energy Concrete for Use in Slip-form Concrete Paving

Principal Investigator: Professor Surendra Shah

A final report submitted to the Infrastructure Technology Institute

Chapter 1

SFSCC: balancing flowability and shape stability

1.1 Quantifying effects of clay on the rheology of cement pastes and the green strength of concretes

Slipform self-consolidating concrete (SFSCC) requires sufficient flowability in order to consolidate without the use of internal vibration. However, this concrete must also gain sufficient green strength in order to keep its shape immediately after slipform paving; a process which involves consolidation and extrusion. It has been demonstrated for minimal compaction energy concrete used in SFSCC that small additions of clays (less than 1% by mass of cement) can make substantial improvements on the shape stability [1]. Clays have also been shown to improve the cohesiveness of cement-based extruded materials at similarly low dosages [2, 3, 4].

The purpose of this study is to quantify how both micro and nanoclay admixtures affect the strength of the cement paste microstructure from a rheological stand point and to compare this to the behavior of fresh concrete. Shear and compressive rheology techniques are used to measure how the solids volume fraction of cement suspensions with different admixtures evolves with stress. Based on these relationships, the effectiveness that different clays and other admixtures have on the balance between flowability and shape stability can be measured. A shear rheology method [5] is used to investigate how the maximum packing fraction of flocs changes under increasing shear stress, while a compressive rheology method [6] is used to determine changes in the local solids volume fraction (solids volume fraction of the sediment region, or sediment volume fraction) under increasing compressive stress. Results are compared to green strength tests performed on concrete mixes derived from the cement paste mixes investigated. Results in this section have been published in [7].

1.1.1 Cement flocculation

When water and cement are combined in typical proportions, the inherent high concentration of the paste leads to the rapid formation of flocs due to the increase in the frequency of particle collisions [8]. During mixing, there is a continuous formation and breakage of flocs. For a constant mixing speed, the floc size will reach an equilibrium that is a function of the flocculation strength; higher flocculation strengths can sustain larger flocs [9]. At sufficiently high mixing rates, the microstructure will reach a maximum solids volume fraction or maximum packing fraction that is a function of the flocculation strength as well as the particle shape and size distribution [10]. For suspensions with

similar particle shapes and size distributions, stronger floc strengths lead to lower maximum packing fractions, which is due to the higher amount of water trapped by the flocs thereby inhibiting efficient packing [11, 12, 13, 14]. Once mixing is complete, the flocs are free to grow, forming a space-filling network capable of supporting stress. The rate at which this occurs depends on both the rate of successful collisions and the rate of breakage due to particle movement arising from Brownian motion and sedimentation [15].

The fresh cement paste microstructure can sustain shear stresses elastically up to the yield stress. The yield stress is dependent on both the flocculation strength and structure of the suspension [16]. When the shear stress exceeds the yield stress, flow is initiated and flocs begin to break down into smaller flocs. This microstructural process releases entrapped liquid within the flocs, increasing the liquid available for lubrication between particles. As a result, the viscosity decreases with increased shear, which explains the shear-thinning behavior of suspensions such as cement pastes [17, 18].

Cement paste responds in a thixotropic manner when shear stresses are applied and removed; flocs break apart under stress leading to a decrease in viscosity, but rebuild over time once the stress is removed due to flocculation, subsequently increasing the viscosity [19]. This reversible property is essential to the fresh state of concrete and has garnered much research in recent years [20, 21, 22, 23, 24, 25]. Thixotropy is especially convenient for applications such as formwork pressure, where the increase in viscosity over time leads to a decrease in formwork pressure [26, 27, 28, 29, 30]. The influence of clays on thixotropy should be assessed in future work, but is not investigated here; the main focus is the effect of clays on floc strength.

The concept of a yield stress exists in suspensions subjected to compression just like suspensions subjected to shear stress. Below the yield stress, a suspension will deform elastically, and when the yield stress is exceeded, the microstructure will irreversibly collapse, where flocs break apart in order to rearrange into a denser configuration. As the flocs break apart, entrapped liquid is released, and the slow migration of water through the dense microstructure results in a viscoelasto-plastic response [31]. This new, denser configuration will in turn have a higher yield stress, since more particles that are tightly configured must rearrange themselves to allow for further consolidation.

1.1.2 Theoretical background for experimental methods

Shear rheology method

In studies by Liu and Soua et al. [5, 9], methods were developed to estimate the relative floc size of highly concentrated suspensions for a given shear stress. For non-flocculated suspensions, the well-known Krieger and Dougherty model [32] relates the viscosity of a suspension to the maximum packing fraction by Equation 1.1:

$$\frac{\eta}{\eta_0} = \left(1 - \frac{\phi}{\phi_m}\right)^{-k}, \tag{1.1}$$

where η is the viscosity of the suspension, η_0 is the viscosity of the suspending medium, ϕ is the total solids volume fraction, ϕ_m is the maximum attainable packing fraction and k is a fitting parameter, usually taken as 2, determined from experiments [10]. Stuble and Sun [11] demonstrated that the Krieger and Dougherty model can be fit for cement pastes, even if the parameters in Equation 1.1 do not take on the same physical meanings as those for non-flocculated suspensions [11, 33]. This model implies that an increase in viscosity is due to an increase in the total solids volume fraction, and furthermore, as $\phi \to \phi_m$, $\eta \to \infty$, reaching solid-like behavior. A convenience of having k fixed at 2 is that the maximum packing fraction can be determined by fitting a straight line to $1 - (\eta/\eta_0)^{-1/2}$ versus ϕ; when $1 - (\eta/\eta_0)^{-1/2} \to 1$, $\eta \to \infty$ and ϕ_m is achieved. However, flexibility is lost in the ability to fit the data to experiments. In order to increase the flexibility, Liu [10] added an adjusting parameter to yield Equation 1.2:

$$\frac{\eta}{\eta_0} = \left[b\left(1 - \frac{\phi}{\phi_m}\right)\right]^{-2} = \left[a\left(\phi_m - \phi\right)\right]^{-2}, \tag{1.2}$$

where the adjusting factor $a = b/\phi_m$. Soua et al. extend this concept to account for flocculated suspensions [5] (in similar fashion to a study by Liu [9]). As flocs form, they begin to trap water, reducing the amount of free water available to lubricate the system. As a result, the viscosity of the suspension increases. In addition, Equation 1.2 does not hold, and the relationship between viscosity and total solids volume fraction becomes a relationship between viscosity and effective total solids volume fraction (total solids volume fraction of the flocs). This effective total solids volume fraction accounts for the increase of entrapped water. Just like non-flocculated systems, the maximum packing fraction of the flocculated system varies with stress for a given floc size.

As the evolving flocs are subjected to increasing shear stress, the flocs will break down in size and continue to do so until the individual particles are achieved. Figure 1.1 demonstrates how the maximum packing fraction of the flocs (ϕ_{fm}) evolves with stress. As the stress increases past the yield stress, the flocs begin to break down and release entrapped water, resulting in a decrease in viscosity. In addition, particles can realign within the flow field to form a tighter configuration [5]. When the stress is sufficiently larger than the yield stress, ϕ_m is achieved and all the entrapped water from the flocs is released. As a result, Equation 1.2 now becomes Equation 1.3 according to Soua et al. [5]:

$$\frac{\eta}{\eta_0} = \left[b\left(1 - \frac{\phi_f}{\phi_{fm}}\right)\right]^{-2} = \left[a'\left(\phi_{fm} - \phi_f\right)\right]^{-2} \text{ for } \tau > \tau_0, \tag{1.3}$$

where ϕ_f is the total solids volume fraction of the flocs, ϕ_{fm} is the maximum packing fraction of the flocs, $a' = b/\phi_{fm}$, τ is the shear stress and τ_0 is the yield stress of the suspension. Note that for $\tau \gg \tau_0$, Equation 1.3 becomes Equation 1.4 (similar to Equation 1.2):

$$\frac{\eta}{\eta_0} = \left[a\left(\phi_m - \phi\right)\right]^{-2} \text{ for } \tau \gg \tau_0. \tag{1.4}$$

In order to determine ϕ_{fm} and ϕ_m, a method developed by Liu can be implemented [10]. Flow curves are obtained for mixes with different total solids volume fractions. For each stress value of each curve, the apparent viscosity, η, is calculated by taking the slope (stress/strain rate), shown in Figure 1.2, marked by the circles for an example stress of 78 Pa. Then, for each stress value, the value $1 - (\eta/\eta_0)^{-1/2}$ is plotted against the corresponding total solids volume fraction. A linear fit is then applied to calculate when $1 - (\eta/\eta_0)^{-1/2} = 1$, at which point, ϕ_{fm} is achieved for that given stress value, as shown in Figure 1.3. Note that the relative viscosity, η_r, is η/η_0. Repeated for each stress value gives a $\phi_{fm} - \tau$ curve. Finally, ϕ_m is the asymptotic limit, ϕ_{fm} value for $\tau \gg \tau_0$ of the curve. For example, Figure 1.4 shows ϕ_{fm}/ϕ_{τ_0} versus τ/τ_0 (where ϕ_{τ_0} is ϕ_{fm} evaluated at $\tau = \tau_0$), for a cement paste representing a flocculated suspension and a cement paste containing a superplasticizer (SP) representing a deflocculated suspension. Although ϕ_m is primarily dependent on the particle shape and size distribution, a flocculated suspension typically shows a lower ϕ_m when compared to a deflocculated system [11, 12, 13, 14], which is demonstrated in Figure 1.4. In addition to the ϕ_m, the difference between ϕ_m and ϕ_{τ_0} (or ϕ_{dif}) is less than the deflocculated mix; that is, the structure experiences less change with increasing stress than the deflocculated mix. This can be considered as another indication of floc strength.

Compressive rheology method

When the yield stress is exceeded in compression, the suspension's network collapses irreversibly, leading to a denser configuration. The increase in the local solids volume fraction (or the solids

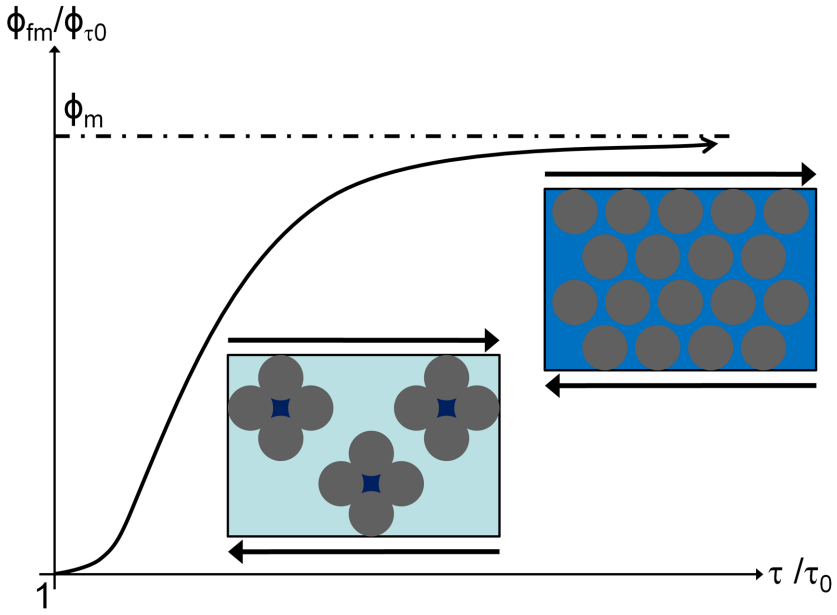

Figure 1.1: Evolution of maximum packing fraction of flocs as a function of stress

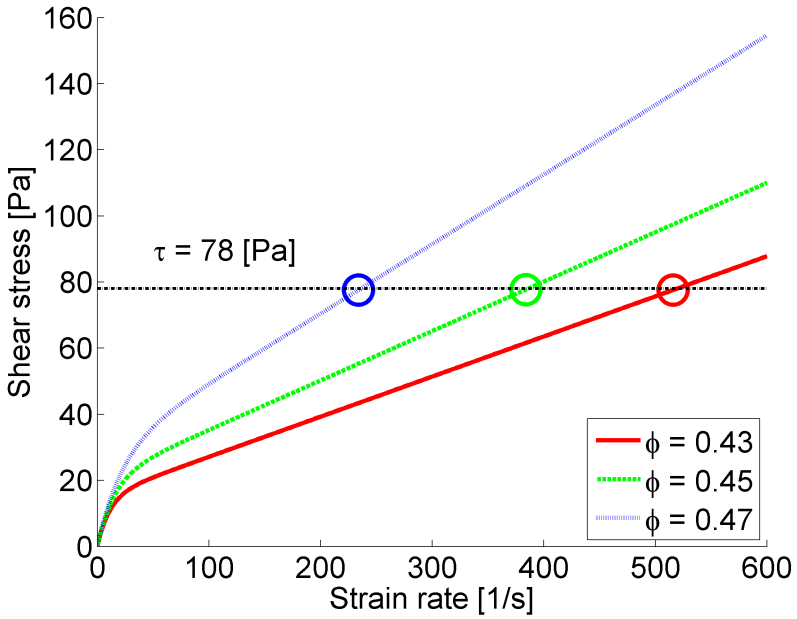

Figure 1.2: Flow curve depicting circles where viscosities are calculated for a given stress value of 78 Pa

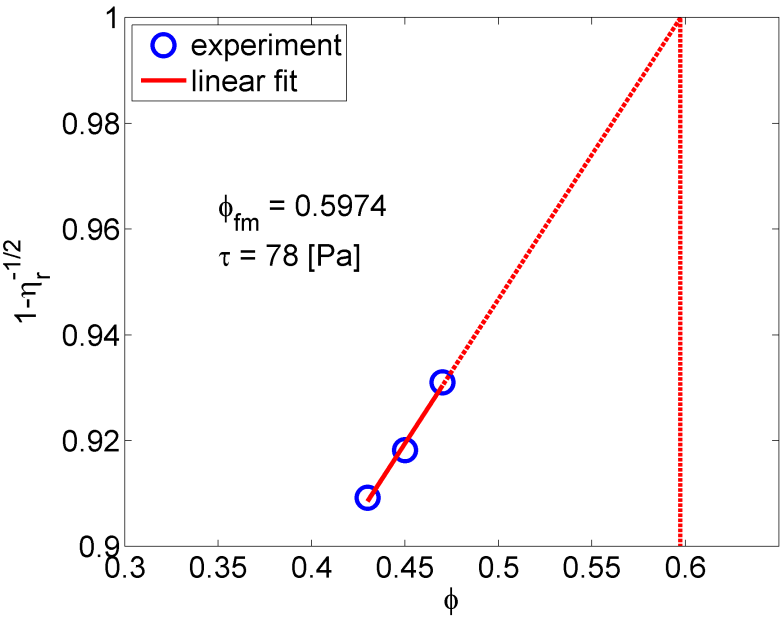

Figure 1.3: Determination of maximum packing fraction of the flocs for a given stress value of 78 Pa

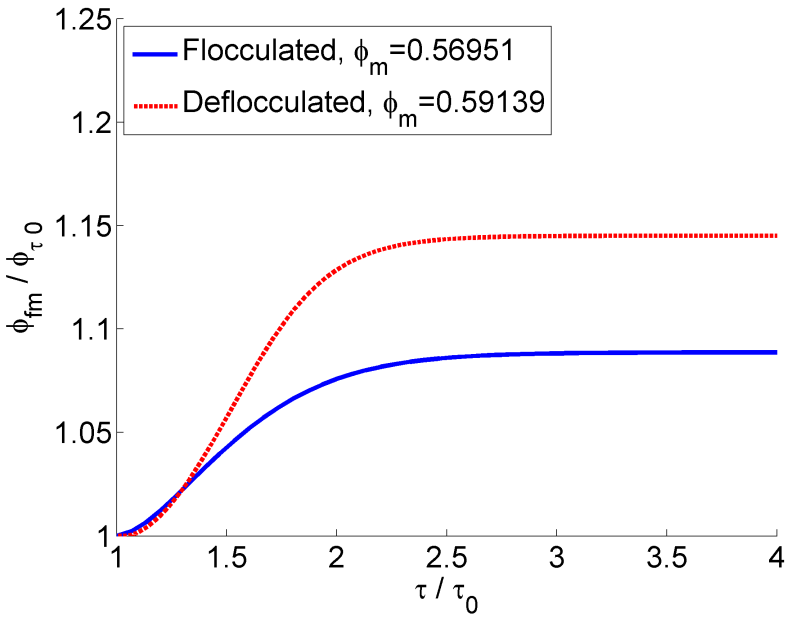

Figure 1.4: Maximum packing evolution as a function of stress for flocculated and deflocculated cement pastes

volume fraction of the sediment region or simply, the sediment volume fraction) results in a higher compressive yield stress in the new configuration, since a denser configuration requires more particles that are tightly packed to rearrange themselves to allow for further consolidation. Thus, the compressive yield stress is a function of the sediment volume fraction and is governed by the particle arrangement and strength of the microstructure. In general, higher number of contact points between flocs or the stronger bonds between flocs will result in a higher yield stress. However, the level of heterogeneity of the microstructure can also play a role (see for example, [34]).

The compressive yield stress can be determined experimentally in several different ways, and in this study, the centrifugal approach is used [6]. In this method, a suspension is subjected to different centrifugal accelerations as sketched in Figure 1.5. At each acceleration, the equilibrium height of the sediment region is recorded. This set of data, along with the density of the solid and suspending fluid, initial sediment volume fraction and centrifuge characteristics are analyzed to determine the compressive yield stress. Both the yield stress and sediment solids volume fraction are solved from Equation 1.5 which is derived from force balance and continuity equations [35]:

$$\frac{d\sigma}{dz} = -\Delta\rho g\phi_0 \left(1 - \frac{z}{R}\right), \tag{1.5}$$

where σ is the compressive stress, z is the distance measured from the bottom of the centrifuge specimen tube, $\Delta\rho$ is the density difference between solid and liquid phases, g is the centrifugal acceleration, ϕ_0 is the initial sediment volume fraction, and R is the distance between the center of the centrifuge and the bottom of the centrifuge specimen tube (see Figure 1.5). Solving this equation requires a numerical integration scheme. The theory is described in [6, 35] while an approximate solution is given in [35]. This approximation (which was used in this study) applies the mean value theorem to the conservation of mass condition, bypassing numerical integrations and cumbersome iterative processes while sacrificing little accuracy [35]. The solution includes equations for the compressive stress and sediment volume fraction at the bottom of the centrifuge tube (Equations 1.6 and 1.7):

$$\sigma_0\left(bottom\right) \approx \Delta\rho\phi_0 H_0 g \left(1 - \frac{H_{eq}}{2R}\right), \tag{1.6}$$

$$\phi\left(bottom\right) \approx \frac{\phi_0 H_0 \left[1 - \frac{1}{2R}\left(H_{eq} + g\frac{dH_{eq}}{dg}\right)\right]}{\left[\left(H_{eq} + g\frac{dH_{eq}}{R}\right)\left(1 - \frac{H_{eq}}{R}\right) + \frac{H_{eq}^2}{2R}\right]}, \tag{1.7}$$

where H_0 is the initial height in the centrifuge tube and H_{eq} is the equilibrium height at the given acceleration. $\sigma_0\left(bottom\right)$, the compressive yield stress at the bottom of the tube, can then be plotted as a function of $\phi\left(bottom\right)$, the sediment volume fraction at the bottom of the tube, for a series of equilibrium heights corresponding to different accelerations. Among many other dense ceramic suspensions, this method has been successfully used for cement mixes [36]. For mixes with similar particle arrangements, a higher compressive yield stress for a particular sediment volume fraction represents a higher flocculation strength as shown in Figure 1.6, where a flocculated suspension (cement paste) is compared to a deflocculated suspension (cement paste containing a SP).

1.1.3 Experimental materials and methods

In this study, six different mix compositions were tested: a cement control mix (CM), a cement-fly ash mix (FAM), a cement-superplasticizer mix (SPM) and three different cement-clay mixes (CM1, CM2, and CM3, containing clays 1, 2 and 3 respectively). General descriptions of the fine materials are shown in Table 1.1, while Figures 1.7 through 1.14 show scanning electron microscope images of the fly ash and clays under different magnifications [37, 38]. All three clays are commercially

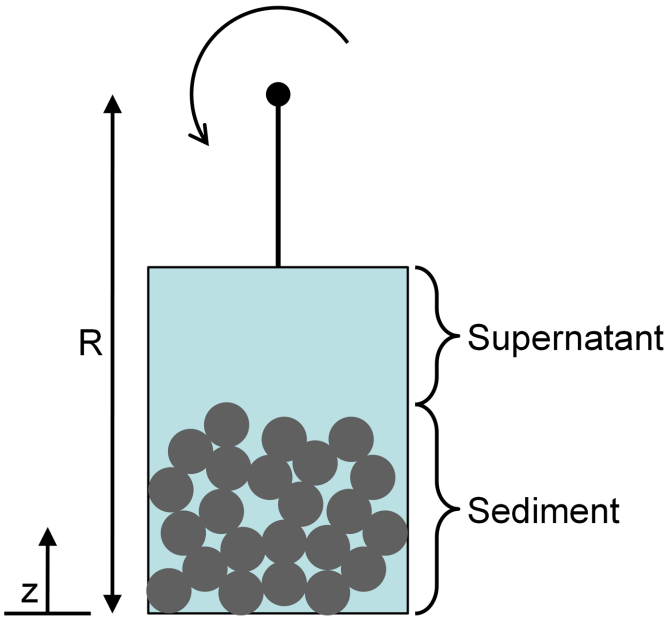

Figure 1.5: Schematic of the centrifuge process

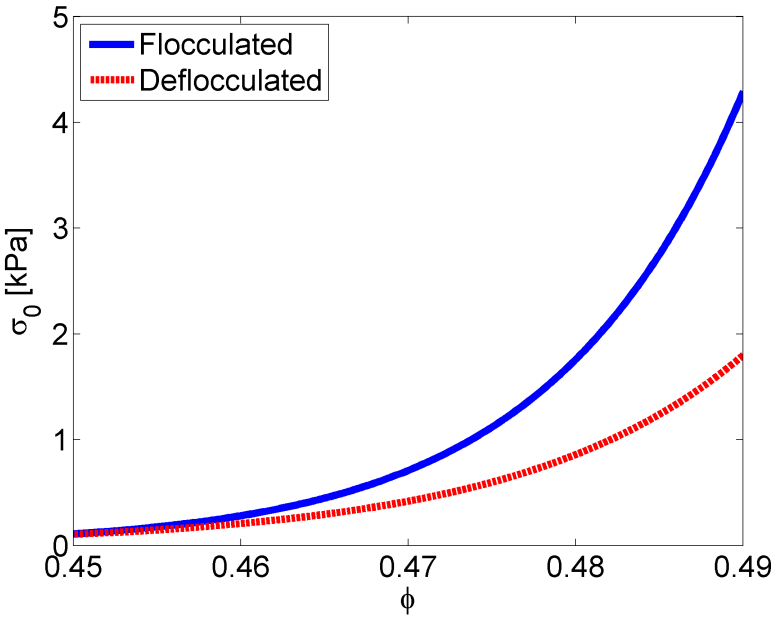

Figure 1.6: Compressive yield stress as a function of the local solids volume fraction for flocculated and deflocculated cement pastes

available. Clay 1, Acti-Gel®, is a highly purified, magnesium alumino silicate. The purification process involves a wet exfoliation of high water-demanding impurities such as smectite [39]. Under shearing, Clay 1 breaks down into needle like structures with lengths on the order of a micron and diameters of several nanometers (see Figure 1.10). Clay 2, Concresol®, is a kaolinite clay that is typically been used to modify rheological behaviors in cement and concrete [40], and has a plate-like structure. Clay 3, MetaMax®, is a metakaolin clay composed of pozzolonic amorphous alumino silicates formed by controlled calcination of kaolinite. The particle size distribution is finer than fly ash particles, yet coarser than silica fume particles, and also has a plate-like structure. This leads to improved reactivity over fly ash and reduced water demand compared to silica fume [41]. Clays such as metakaolin have frequently been incorporated into cement-based materials in order to improve hardened state properties such as strength and durability [42, 43, 44, 45, 46, 47, 48]. Metakaolin specifically is used due to its pozzolanic characteristics; typical dosages in concrete range from 10-30% by mass of cement replacement [42, 43, 44, 45, 46, 47, 48]. However in this study, clays have been added from 0.5 to 1.5% by mass of cement to affect the fresh state. The chemical compositions of each fine material are given in Table 1.2, while the particle size distribution for each fine material is given in Figure 1.15. In addition to the fine materials, a naphthalene-based SP, Daracem 19® [49], was also used. This particular generation of SP was chosen for two reasons. First, the SP only affects the chemistry of the cement through electrostatic repulsion, and second, naphthalene-based SPs have been shown not to be highly absorbed onto clays in comparison to their polycarboxylate-based counterparts.

Table 1.1: Description of fine materials

Material	Specific gravity	Mean particle size [μm]	Specific surface area [m^2/g]	Water absorbtion [%]	Description	Source
Cement	3.15	14.8	1.40		Type I	[50, 51]
Fly ash	2.72	23.5	0.958		Class C	[52, 53, 54]
Clay 1	2.62	65.2, 1.75*	150	200	Purified magnesium alumino silicate	[39, 55]
Clay 2	2.65	13.0, 0.50*	23	65	Kaolinite, illite, quartz	[40, 56]
Clay 3	2.50	3.54, 1.20*	13	50	Purified, calcined metakaolin	[41, 54, 57]

*Highly dispersed state

Table 1.2: Fine material chemical compositions

Chemical composition [%]	Cement [51]	Fly ash [52]	Clay 1 [39]	Clay 2 [40]	Clay 3 [54]
SiO_2	19.5	33.15	49.57	68.0	53.00
Al_2O_3	4.7	17.89	9.44	24.0	43.80
Fe_2O_3	2.80	6.06	3.31	2.4	0.43
CaO	64.2	26.09	1.88	0.2	0.02
MgO	2.50	5.84	8.81	0.5	0.03
SO_3	2.6	1.39	0.00	0.0	0.03
Na_2O	0.0	2.64	0.59	0.1	0.23
K_2O	0.0	0.40	0.66	2.2	0.19
TiO_2	0.0	0.00	0.42	1.7	1.70
P_2O_5	0.0	0.00	0.68	0.0	0.03
MnO	0.0	0.00	0.02	0.0	0.00
CrO_3	0.0	0.00	0.02	0.0	0.00

1.1.4 Mix designs and mix protocol

Concerning the shear rheology method, three different total solids volume fractions were required to determine the maximum packing fraction relationship: 0.43, 0.45 and 0.47. These values were chosen to be centered around a total solids volume fraction of 0.45 for comparison to the centrifuge results. For the compressive rheology method, all mixes had the same total solids volume fraction of 0.45, which corresponds to a w/b (water-to-binder ratio) of about 0.39 for the cement control mix. The binder is considered the sum of the cement and the class-C fly ash. The mix designs are shown in Tables 1.3 through 1.5, while the mixing protocol is shown in Table 1.6. A small planetary mixer was used. It is noted that the dry ingredients were mixed first in order to achieve proper dispersion of the mineral admixtures before the water was added. For dense suspensions such as cement pastes, flocculation occurs rapidly, which can hinder proper dispersion before the microstructure is tested.

1.1.5 Shear rheology experimental method

A temperature controlled Haake Rheostress 150® rheometer with a concentric-cylinder geometry was used to determine the flow curves for the shear rheology method. The protocol involved a two minute pre-shear at 1100 1/s followed by two minutes of rest. The strain rate was then increased gradually over ten minutes to a final value of 1000 1/s. Flow curve results consisted of shear stress versus strain rate curves. This was performed for each total solids volume fraction three times for each composition. From this data, only the strain rate range of 0-200 1/s was used to determine the

Table 1.3: Mix designs for a volume fraction of 0.43 and a volume of one liter for the shear rheology method

Material	CM	SPM	FAM	CM1	CM2	CM3
Cement [g]	1350.	1350.	852.	1334.	1334.	1334.
Water [g]	570.	564.	570.	570.	570.	570.
Admixture [g]	0.	6.8	365.	13.3	13.3	13.3

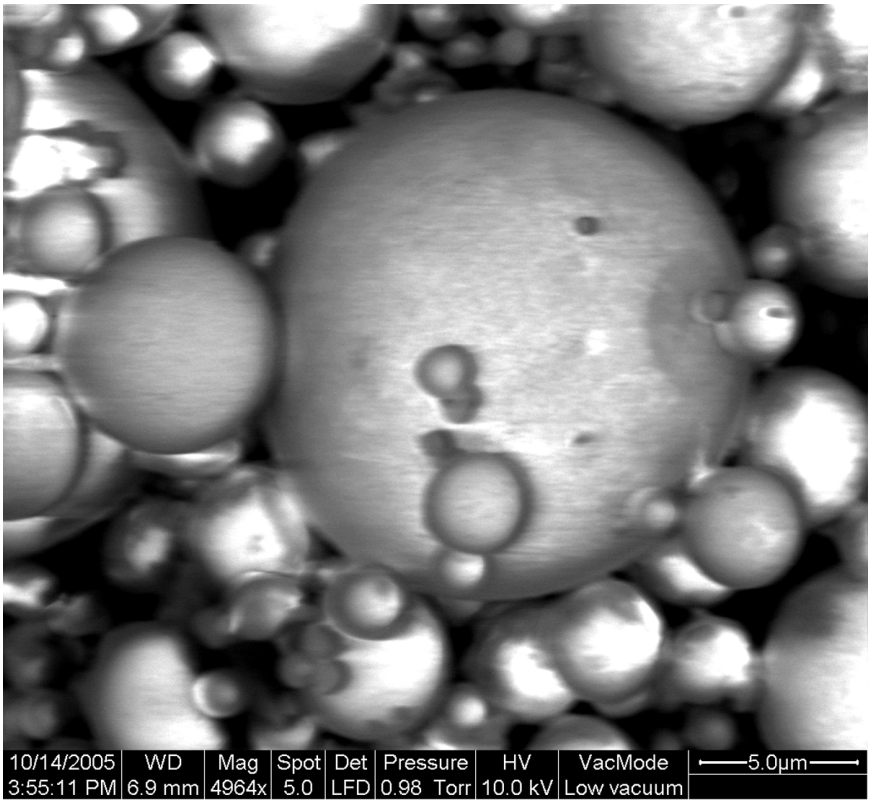

Figure 1.7: Scanning electron microscopy image of fly ash particles [38]

Table 1.4: Mix designs for a volume fraction of 0.45 and a volume of one liter for the shear and compressive rheology methods

Material	CM	SPM	FAM	CM1	CM2	CM3
Cement [g]	1413.	1413.	891.	1396.	1396.	1396.
Water [g]	550.	544.	550.	550.	550.	550.
Admixture [g]	0.	7.1	382.	14.0	14.0	14.0

Table 1.5: Mix designs for a volume fraction of 0.47 and a volume of one liter for the shear rheology method

Material	CM	SPM	FAM	CM1	CM2	CM3
Cement [g]	1476.	1476.	931.	1458.	1457.	1458.
Water [g]	530.	524.	530.	530.	530.	530.
Admixture [g]	0.	7.4	399.	14.6	14.6	14.6

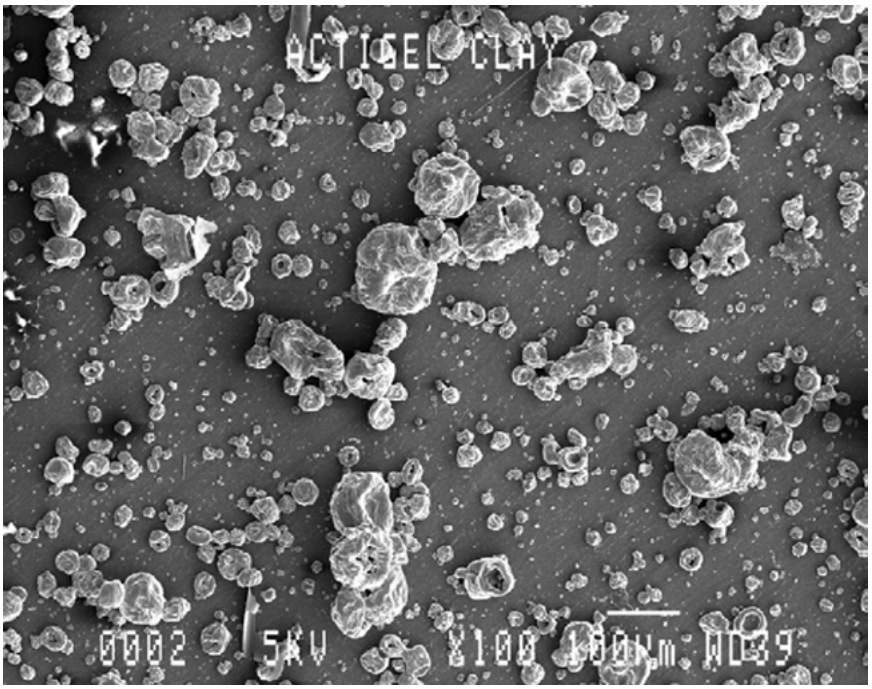

Figure 1.8: Scanning electron microscopy image of Clay 1 particles (low magnification) [37]

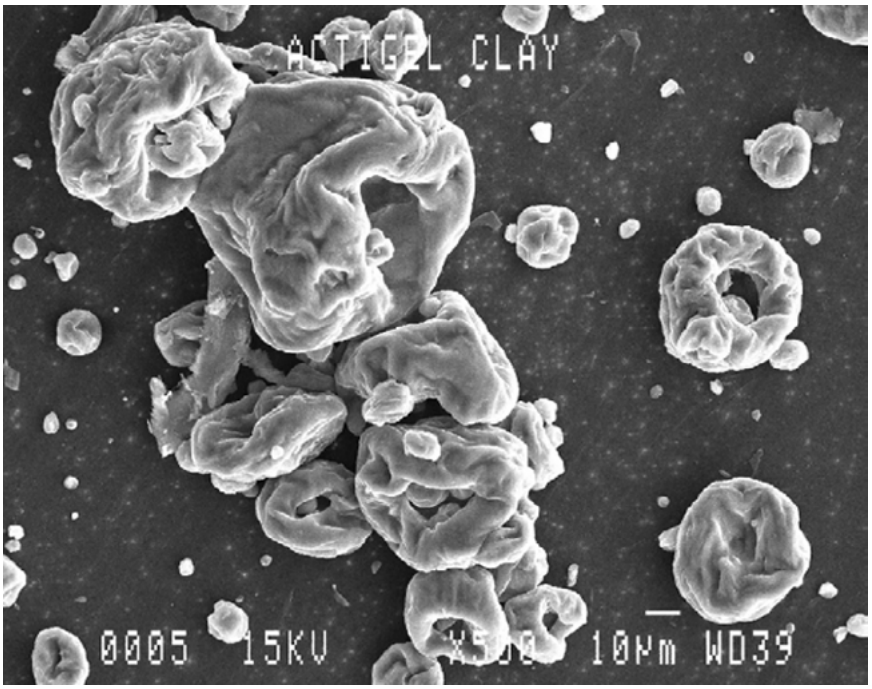

Figure 1.9: Scanning electron microscopy image of Clay 1 particles (high magnification) [37]

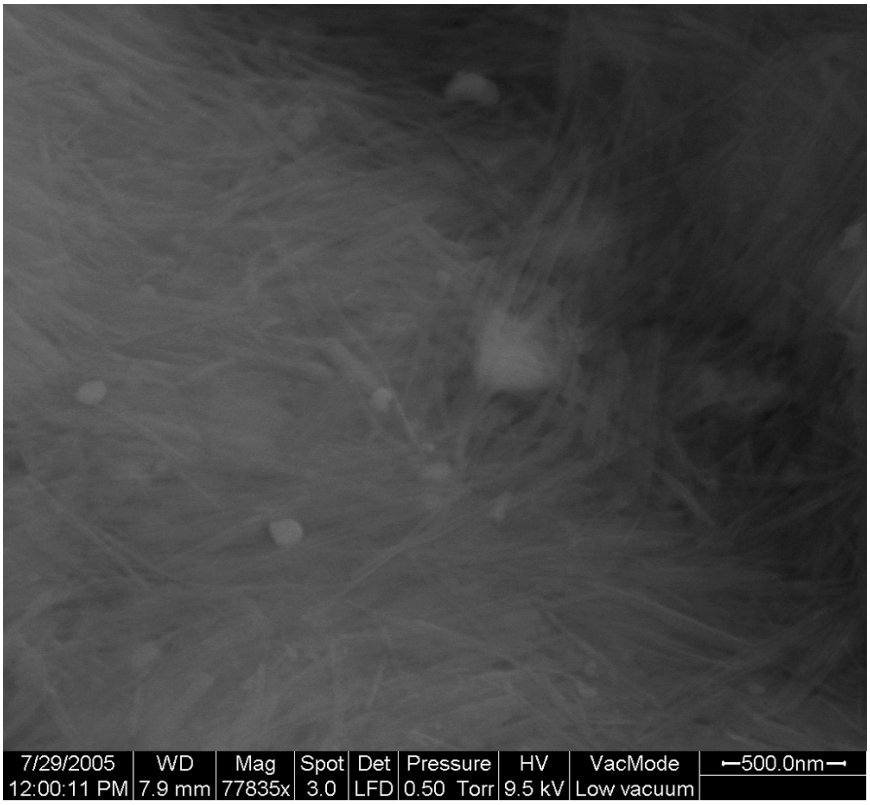

Figure 1.10: Scanning electron microscopy image of Clay 1 particles (very high magnification) [38]

Table 1.6: Cement paste mixing protocol using a small planetary mixer

Time [mm:ss]	Task
0:00	Mix dry materials at low speed
1:00	Add water and SP and mix at low speed
3:00	Stop to scrape sides of mixer
4:00	Mix on high speed
6:30	Stop to scrape sides of mixer
7:30	Mix on high speed
10:00	Perform tests

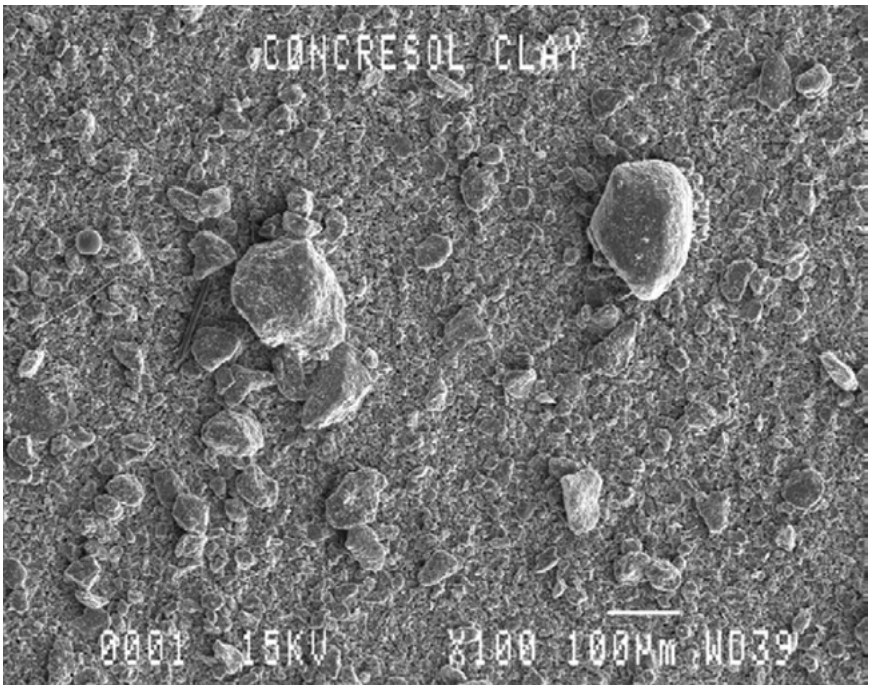

Figure 1.11: Scanning electron microscopy image of Clay 2 particles (low magnification) [37]

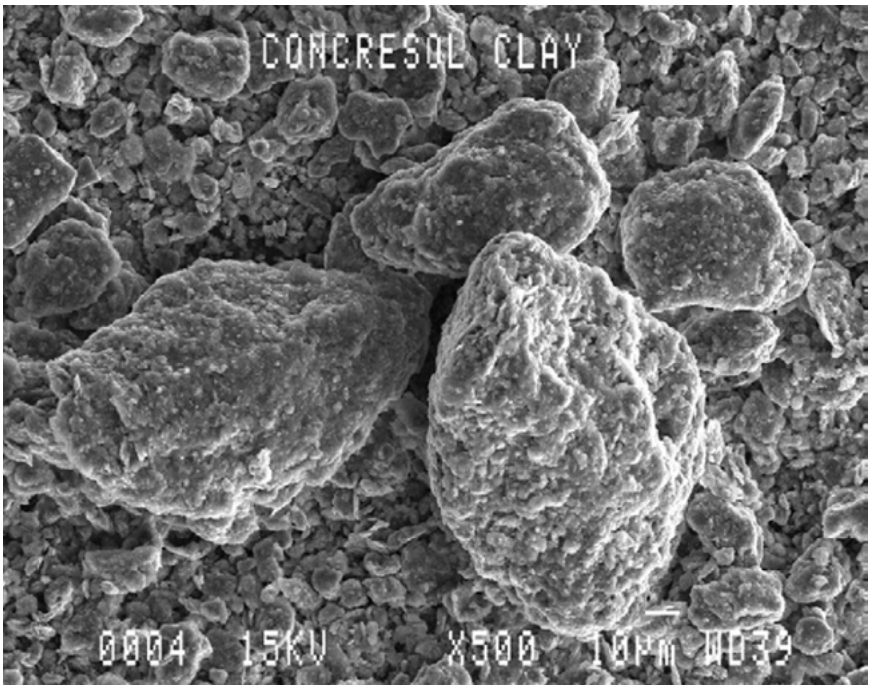

Figure 1.12: Scanning electron microscopy image of Clay 2 particles (high magnification) [37]

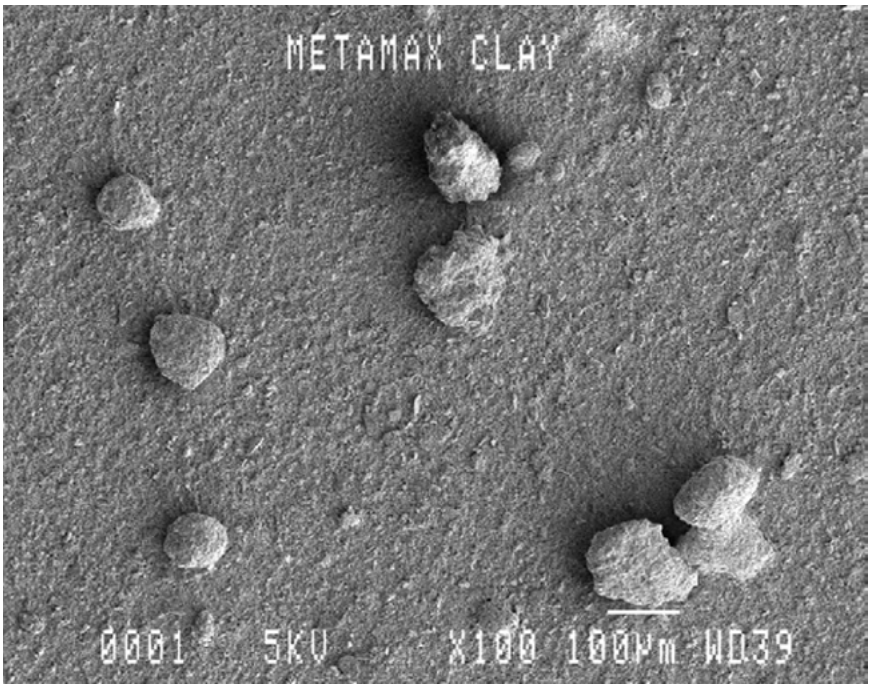

Figure 1.13: Scanning electron microscopy image of Clay 3 particles (low magnification) [37]

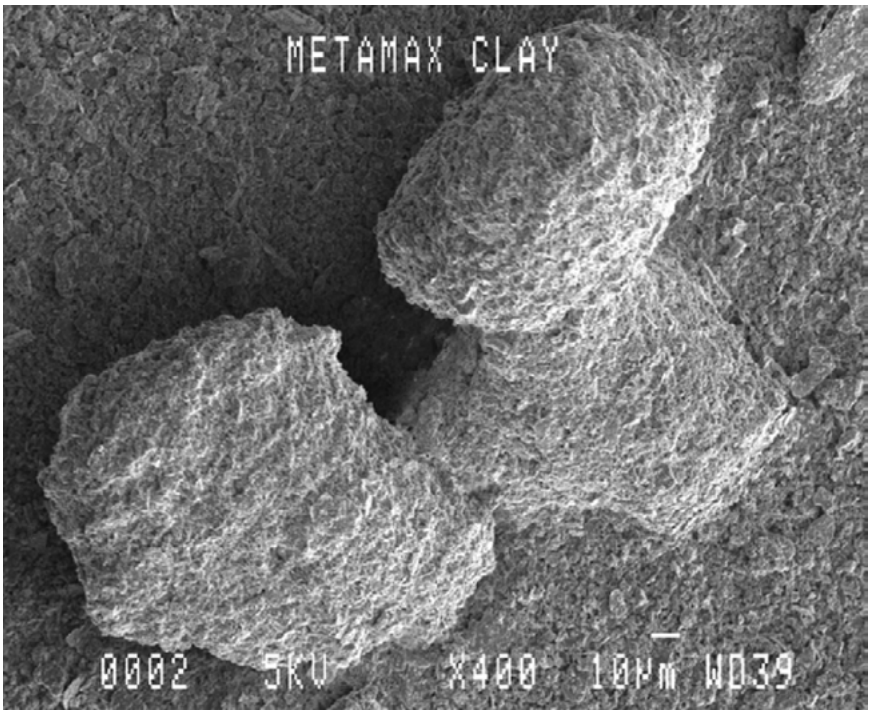

Figure 1.14: Scanning electron microscopy image of Clay 3 particles (high magnification) [37]

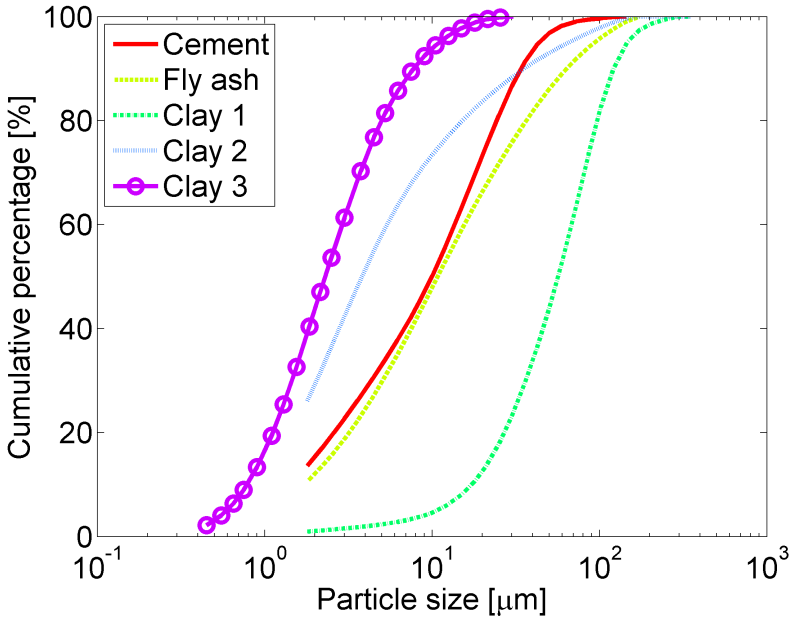

Figure 1.15: Particle size distributions for fine materials [38]

maximum packing evolution. $1-(\eta/\eta_0)^{-1/2}$ versus ϕ was plotted and these curves were extrapolated to 1 for each shear stress in order to determine the maximum packing fraction. The ϕ_{fm} relationship was then constructed to find ϕ_m. The yield stress of each composition was determined using the full flow curve (strain rate range of 0-1000 1/s). The entire flow curved was used to ensure that a proper curve fit could be accomplished. A modified Bingham law was used to fit the data, and since all materials exhibited shear-thinning over a large range of strain rates, the entire curve was used so that the Bingham parameters had their proper meaning. In evaluating the maximum packing fraction, only the initial strain rate range was considered since this range is typically experienced in the field.

1.1.6 Compressive rheology experimental method

A SORVALL ® RC 5B Plus superspeed centrifuge was used to determine the compressive yield stress as a function of the sediment volume fraction. In order to achieve a flat bottom, the round-bottom centrifuge tubes were filled with a structural epoxy. After mixing, four samples of the same batch were centrifuged simultaneously for 20 minutes at a particular speed. This duration was determined to be the minimum time required to ensure that the equilibrium state was achieved for all rotational speeds considered. Equilibrium heights were obtained for rotational speeds ranging from 2000 to 10000 rpm for each specimen, which corresponds to approximately 1-1000 g. Not all rotational speeds could be performed on the same batch before the cement pastes would begin to show the effects of hydration. It was determined that batches could be subjected to three different rotational speeds, and conducting three rotational speeds produced the same results as performing each speed individually. Consequently, each batch was subjected to a set of three rotational speeds: 2000, 5000, 8000; 3000, 6000, 9000; or 4000, 7000, 10000 rpms. The rotational speeds were staggered as such to minimize bias. An example of the raw data is shown in Figure 1.16, along with a theoretical fit. A

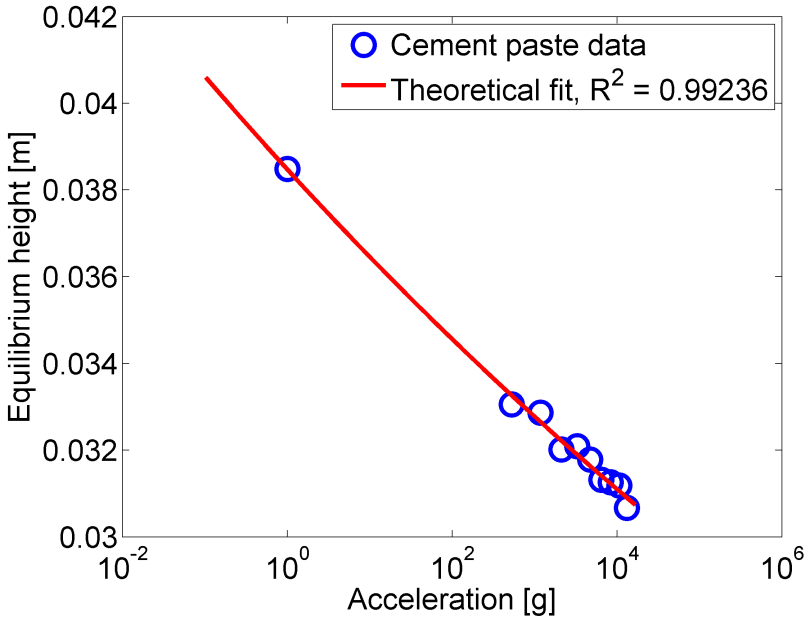

Figure 1.16: Raw data from the centrifuge for the cement control mix along with a logarithmic fit

regression analysis was performed to fit the data to an equation of the form:

$$\ln H_{eq} = a_1 + a_2 + \ln g + a_3 \left(\ln g\right)^2, \tag{1.8}$$

as recommended by Green et al. [35], where the values a_1 through a_3 are the fitting parameters. From the data collected, Equations 1.6 and 1.7 were used to determine the compressive yield stress.

1.1.7 Determination of green strength

In addition to the two rheology methods, the green strength or strength immediately after casting was determined. These tests were performed on concrete compositions derived from the cement pastes used in the previous tests. A coarse aggregate to fine material ratio of 1.75 and a fine aggregate to fine material ratio of 1.54 were used for all concrete mixes. The coarse aggregate consisted of a round pea gravel with a maximum size of 9.5 mm (0.37 in) while the fine aggregate consisted of a river sand with a maximum size of 4.75 mm (0.187 in). After using the concrete mixing protocol shown in Table 1.7, a 102 × 203 mm (4 × 8 in) cylinder was filled with concrete and then subjected to twenty-five drops on a drop table shown in Figure 1.17. These drops represent external energy that helps consolidate the mix. After consolidation, the fresh concrete was demolded and a bucket was placed on top of the fresh concrete cylinder. Sand was slowly added until the cylinder collapsed. This load was then converted to green strength by dividing by the original cross section. This process was repeated three times for each composition and is demonstrated in Figure 1.17.

1.1.8 Rheology and green strength results

Flow curves for each mix were fit according to a modified Bingham law [58]:

Table 1.7: Concrete mixing protocol using a large planetary mixer

Time [mm:ss]	Task
0:00	Mix dry materials including small aggregate at low speed
1:00	Add water and SP and mix at low speed
3:00	Stop to scrape sides of mixer
4:00	Mix on high speed
6:30	Stop to scrape sides of mixer
7:30	Mix on high speed
10:00	Mix in coarse aggregate on high speed
12:00	Perform tests

Figure 1.17: The green strength test

Table 1.8: Shear rheology results

Composition	τ_0 [Pa]	ϕ_{τ_0}	ϕ_m	ϕ_{dif}
CM	76.32	0.523	0.570	0.0465
SPM	62.24	0.516	0.591	0.0750
FAM	34.76	0.494	0.579	0.0853
CM1	97.31	0.520	0.546	0.0255
CM2	80.65	0.522	0.549	0.0268
CM3	89.02	0.516	0.556	0.0397

$$\tau = \tau_0[1 - exp(-3\frac{\dot{\gamma}}{\dot{\gamma}_{crit}})] + \mu\dot{\gamma}, \tag{1.9}$$

where τ is the shear stress, τ_0 is the yield stress, μ is the plastic viscosity, $\dot{\gamma}$ is the strain rate and $\dot{\gamma}_{crit}$ is the critical strain rate dividing the linear dependence of stress on the strain rate with the nonlinear portion. A modified Bingham equation was used because of its consistent ability to fit the experimental data. Table 1.8 gives the yield stress for the $\phi = 0.45$ compositions, ϕ_{τ_0}, ϕ_m and ϕ_{dif}. Figure 1.18 shows the percent difference between these values as compared to the CM. It can be seen that all the mixes have relatively the same ϕ_{τ_0}, which is reasonable since only small dosages of additives were used except in the case of the FAM (which has the largest difference compared to the CM). However, yield stresses for the SPM and the FAM are lower than the CM while the CM1-3 are higher. This may indicate that although the compositions have similar structures, the bonds between flocs may be weaker for the SPM and the FAM, and stronger for the CM1-3. As the stress increases, both ϕ_m and ϕ_{dif} are larger for the SPM and the FAM but smaller for the CM1-3. This also indicates larger floc strengths for mixes containing clays, and smaller floc strengths for mixes containing superplasticizer or fly ash since the microstructures of the clay mixes do not change as much under stress. Figure 1.19 shows ϕ_{fm}/ϕ_{τ_0} versus τ/τ_0 for all the compositions with their ϕ_m values listed. As noted by both Struble and Sun as well as Mansoutre et al., the maximum packing fraction increases with stress indicating a break down of the structure and realignment of the flocs with respect to the flow field [11, 14]. Graphically, it is shown that the clay mixes do not change as much as the SPM and the FAM, again indicating higher floc strengths.

Struble and Sun used the traditional method of determining ϕ_m by fitting the Krieger and Dougherty model [32] to $\phi - \mu$ data. They reported ϕ_m values of 0.76 and 0.64 for cement pastes with and without SPs, respectively [11]. In this study, cement pastes with and without SPs produced ϕ_m values of 0.59 versus 0.57. The difference in magnitudes may be due to different chemical compositions and particle size distributions. As for the smaller difference between the cement paste with and without SPs, the most likely reason is that the superplasticizer mix was not fully dispersed as in the case for Struble and Sun [11]. As a further comparison, Mansoutre et al. also used a method similar to Struble and Sun to determine ϕ_m for C_3S pastes (the main reactive component in cement) and found ϕ_m to be around 0.45 [14].

The results for the compressive rheology method are shown in Figure 1.20 as the relationship between the sediment volume fraction and compressive yield stress. Both the SPM and the FAM are more compressible compared to the CM. On the other hand, the CM1-3 all show a higher compressive yield stress than the CM. This further suggests the increase in floc strength of the CM1-3 while a decrease in the floc strength for the SPM and the FAM.

Naphthalene-based SPs have been shown to increase the magnitude of the repulsive potential, resulting in weaker flocs [59, 60, 61, 62]. Because the flocs are held loosely together, they can be easily broken down and rearranged under both shear and compressive forces. Using a different compressive

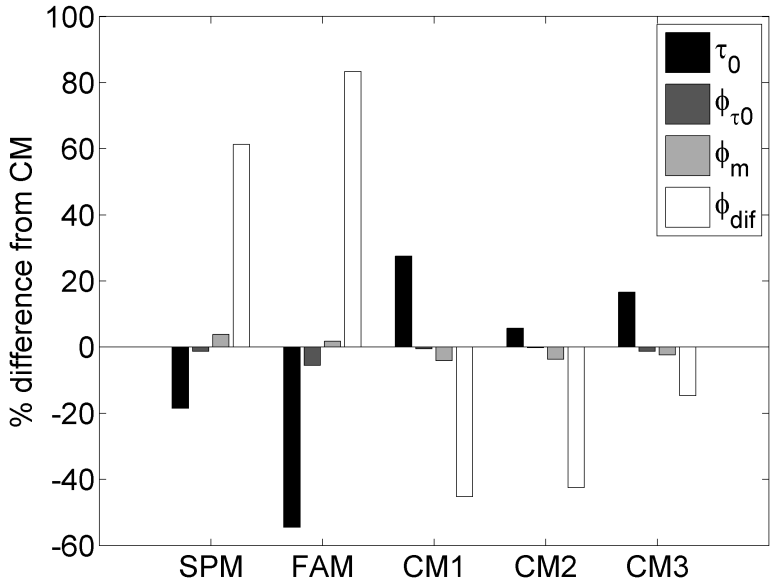

Figure 1.18: Comparison of shear rheology results as compared to the control cement mix

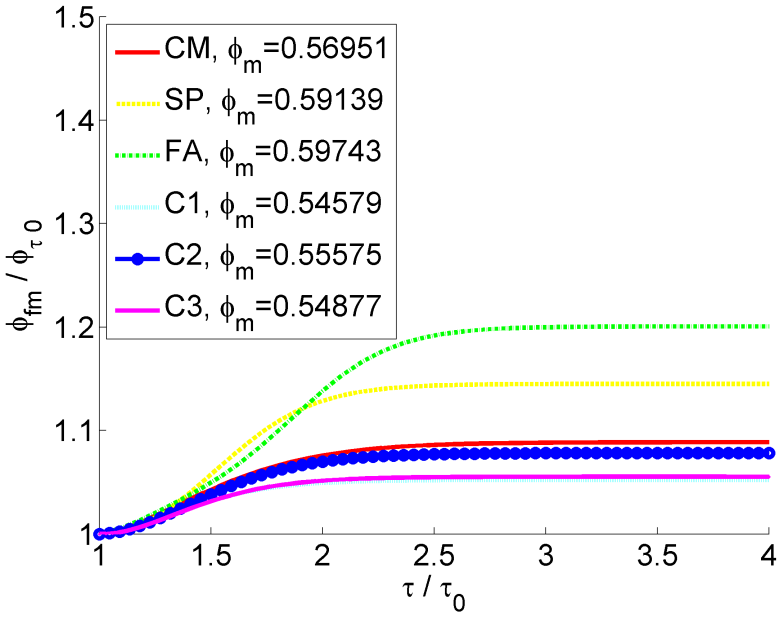

Figure 1.19: Maximum packing densities as a function of stress

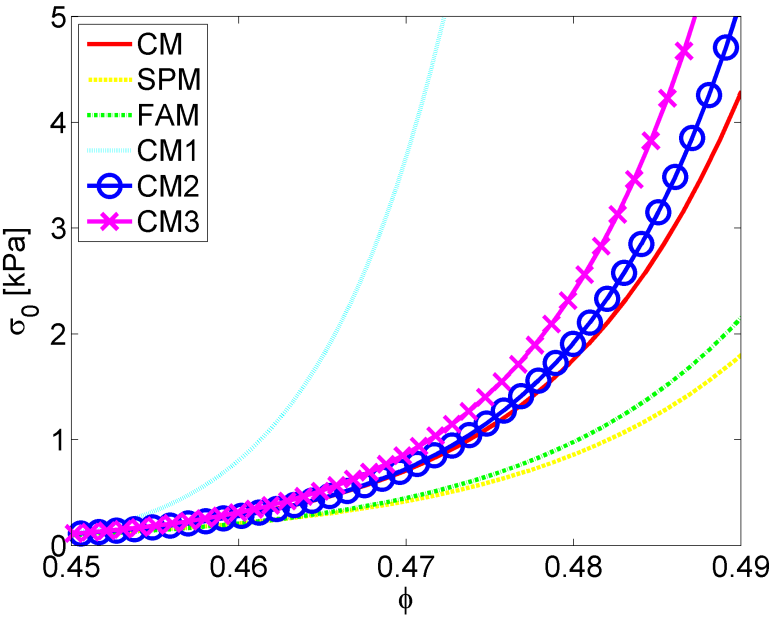

Figure 1.20: Compressive yield stress as a function of sediment volume fraction

yield stress method (but capable of giving similar results to the centrifuge method used in this study [63]), Kjeldsen et al. demonstrate how SPs in general reduce the compressive yield stress because of electrostatic and steric repulsion [62]. For the fly ash mix, improvements in flowability are usually attributed to the shape of the fly ash particles (see Figure 1.7). The spherical shape of the fly ash particles minimizes the surface area to volume ratio thus decreasing water demand. In addition, it is usually noted that the spherical shape acts as a ball bearing, allowing particles to easily roll over each other when rearrangement of the microstructure is required [64, 65, 66, 67, 68]. This would explain the low compressibility. Under high shear stresses, the fly ash can still achieve maximum packing fractions since the spherical shape and low water demand allow efficient flowability even within tight configurations. When comparing the fly ash mix with the rest of the mixes used in the study, it should be noted that the microstructure of the fly ash mix may have a different particle size distribution since a large amount of cement was replaced with fly ash, whereas only small amounts of admixtures were used in the other compositions.

Both the shear and compressive rheology methods indicated that the clays increased the flocculation strength of the cement pastes. One possible explanation of the larger floc strength is that the clays are absorbing water that would normally help lubricate the microstructure and allow particles to easily slide past each other during shear or compression. In the absence of this lubricating water, the suspension would have a higher shear and compressive yield stress. Yet, clays used in this study have all been processed to remove major impurities that are typically responsible for swelling usually associated with natural clays. In addition, the small clay dosages considered would further reduce the amount of water absorbed. Water absorption of the clays could also increase the capillary suction, leading to higher green strengths, as well. In this scenario, only very small reductions in the local relative humidity are necessary to produce large suction pressures [69]. Thus, even small amounts of water absorbed by the clays may explain the influence of clays on shape stability.

Another possibility is that the smaller clay particles are filling the interstices created by the

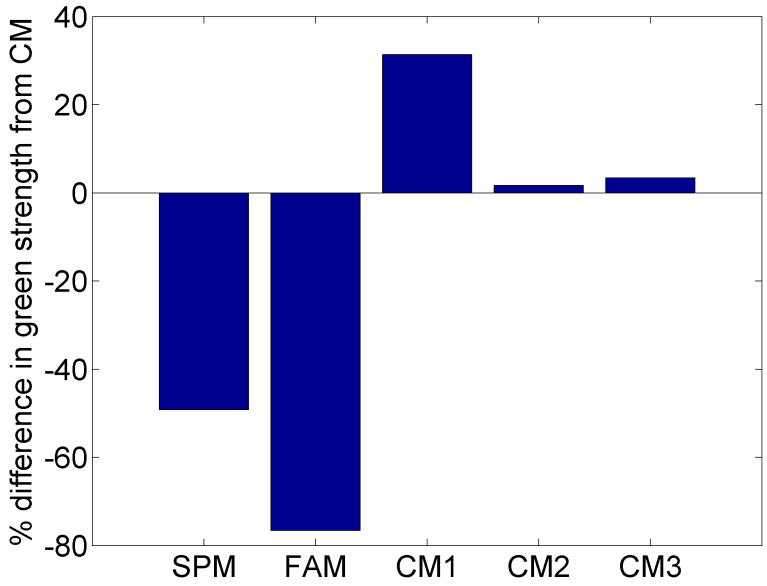

Figure 1.21: Green strength of compositions as compared to the control cement mix

larger cement particles. The number of physical contact points would increase leading to a larger compressive yield stress. However, a 1% addition of any clay type would not significantly improve the compressive strength. In other words, the small addition of clay does not dramatically change the geometry of the floc arrangement (also noted by the similar ϕ_{τ_0} values). Lastly, the clays may be influencing the pore chemistry of the cement paste. Changes in the conductivity and pH can results in lower repulsive van der Waals forces, which may increase the flocculation strength. The exact nature of how clays increase the flocculation strength of cement paste was not within the scope of this research.

The shape stability of each fresh concrete composition is shown in Figure 1.21 and Table 1.9 as determined by the green strength. The results are shown as the percent differences from the green strength of the CM. Both the SPM and FAM experienced a decrease in the green strength compared to the CM. On the other hand, all of the clay mixes had increased green strength with Clay 1 having the largest effect.

1.1.9 Summary

Both shear and compressive rheologies can give helpful insight into how green strength is affected by different admixtures. Agreement was found between both shear and compressive rheologies and green strength tests performed on cement pastes and concretes. The results show how both SP and fly ash decrease the shear and compressive strength while the clays increase the shear and compressive strength. Clays showed a lower maximum packing fraction as well as a smaller change in packing fraction while the SPM and FAM showed opposite trends. It was shown that Clay 1, a purified magnesium alumino silicate clay, was most effective by mass in improving the shape stability.

Table 1.9: Green strength results

Mix	Green strength [kPa]
CM	14.8
SPM	7.5
FAM	3.5
CM1	19.4
CM2	15.0
CM3	15.3

1.2 Investigating effect of clay dosage on rheology, green strength and SFSCC paving applicability

This section aims to investigate the effect of different dosages of different micro and nanoclays to produce SFSCC compositions with the highest green strength without sacrificing the required flowability. This was approached from three different tests: a micro-level analysis investigating the compressive yield stress, a macro-level analysis investigating the green strength, and an applicability test involving a laboratory-scale paving test. A portion of the results in this section has been published in [70].

1.2.1 Experimental methods and materials

In this section, four main mix designs were tested: a cement control mix containing both a naphthalene based superplasticizer and a class C fly ash (designated modified-CM, MCM), and three different cement-clay mixes (designated modified-CM1-3, or MCM1-3). All materials were consistent with those used in the previous section. Only the compressive yield stress and green strength methods described previously were used in this section to determine the effects of clay dosages. For the green strength tests, a larger drop table was used as shown in Figure 1.22 due to the size of the larger aggregates.

Concerning the compressive rheology tests, all compositions had the same initial solids volume fraction of 0.45, which corresponds to a w/b of about 0.43 for the CM mix. The mix compositions for the cement compositions are shown in Table 1.10, while the mixing protocol for both the cement and concrete mixes have been previously described in Tables 1.6 and 1.7. Mixes are designated by the type (MCM or MCM1-3) and the addition of clay (0.5, 1.0 and 1.5% by mass of binder). For the concrete mixes derived from the paste mixes, a coarse aggregate to fine material ratio of 1.75 and a fine aggregate to fine material ratio of 1.54 were used. The coarse aggregate consisted of a limestone gravel with a maximum size of 25 mm (1.0 in) while the fine aggregate consisted of a river sand with a maximum size of 4.75 mm (0.187 in). A small planetary mixer was used for the cement pastes while a large rotary drum mixer was used for the concrete.

1.2.2 Clay dosage effects on compressive rheology and green strength

The compressive yield stress is plotted against the sediment volume fraction for each addition rate (0.5, 1.0 and 1.5% by mass of cement) for each clay in Figures 1.23 through 1.25. All of the clays increase σ_0 over the range of ϕ shown. However, MCM1 shows a higher increase as highlighted in Figure 1.26, which compares all clays at an addition of 1.0% by mass of cement to MCM. Figures 1.23 through 1.25 also show the optimal dosage as 1.0% for each clay. Any additional clay decreases σ_0 (as high as 3% by mass of cement has been investigated [38]). Kuder and Shah also report

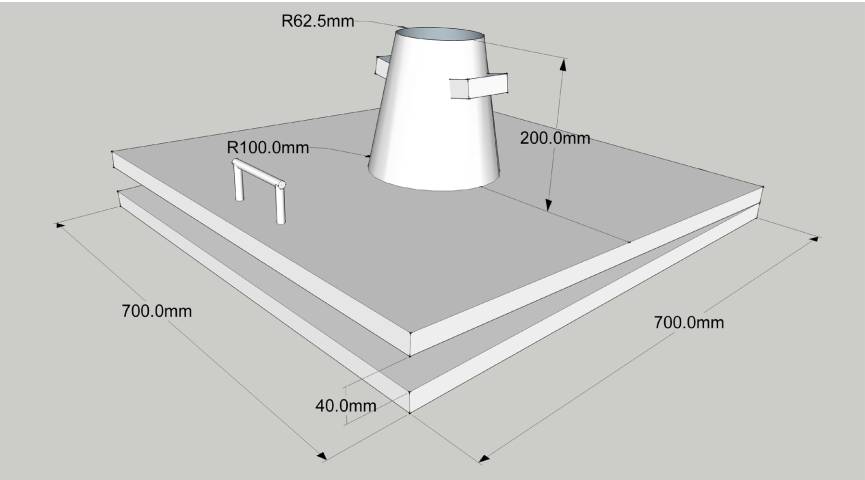

Figure 1.22: Large drop table used to determine green strength of concrete mixtures with large aggregates

Table 1.10: Cement mix compositions for compressive rheology tests for one liter of paste

Mix	Cement [g]	FA [g]	Water [g]	SP [g]	Clay addition [g]
MCM	891.	382.	545.	6.4	0.
MCM1-05	887.	380.	545.	6.3	6.3
MCM1-10	882.	378.	545.	6.3	12.6
MCM1-15	877.	376.	545.	6.3	18.8
MCM2-05	886.	380.	545.	6.3	6.3
MCM2-10	881.	378.	545.	6.3	12.6
MCM2-15	877.	376.	545.	6.3	18.8
MCM3-05	886.	380.	545.	6.3	6.3
MCM3-10	881.	378.	545.	6.3	12.6
MCM3-15	877.	376.	545.	6.3	18.8

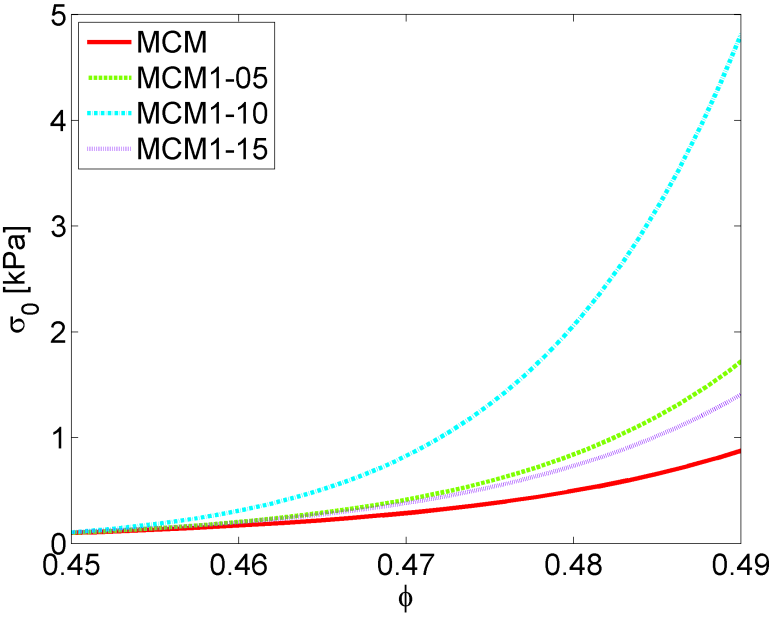

Figure 1.23: Compressive yield stress as a function of sediment volume fraction for Clay 1 at dosages of 0.5, 1.0 and 1.5% by mass of cement compared to the modified control mix

similar optimal dosages of clays for extrusion applications [3]. The reasons for this optimum are still unknown. Comparing these results to the results in the previous section highlight the combined influence of SP, fly ash and clays. It is clear that clays still are able to increase the compressive yield stress even in the presence of SP and fly ash.

In addition to the rheology methods, the green strength or strength immediately after casting was determined. These tests were conducted on concrete mixes derived from the cement pastes used in the previous tests. Green strength results are shown in Figure 1.27. Similar to the compressive yield stress results, the clays improve green strength. In addition, MCM1 performs better than both MCM2 and MCM3 at each dosage amount. Optimal dosages are seen for 1.0% by mass of cement for all clays.

1.2.3 Testing applicability of SFSCC mixes using the minipaver

Finally, a model laboratory minipaver was used on select mixes to demonstrate the applicability of each mix. A model paver, or minipaver, initially developed by Iowa State University [1, 71] was built as shown in Figure 1.28. A schematic of how the minipaver functions is given in Figure 1.29. Immediately after mixing, the fresh concrete is first loaded in the upper level of the minipaver. The concrete is then moved into the vertical shaft and form channel until the stopping plate is reached. This stopping plate forms the front vertical edge of the slab. Without external vibration, the minipaver was pulled by a nylon rope at a constant speed of approximately 0.5 m/min (1.6 ft/min). While the minipaver moves forward, the fresh concrete passes through the form channel and is consolidated by static vertical pressure exerted by the weights in the minipaver. The pressure is applied continuously and uniformly over the length of the form channel, which is accomplished by a slight decrease in channel size. After the end of the slipform casting process, a successful concrete

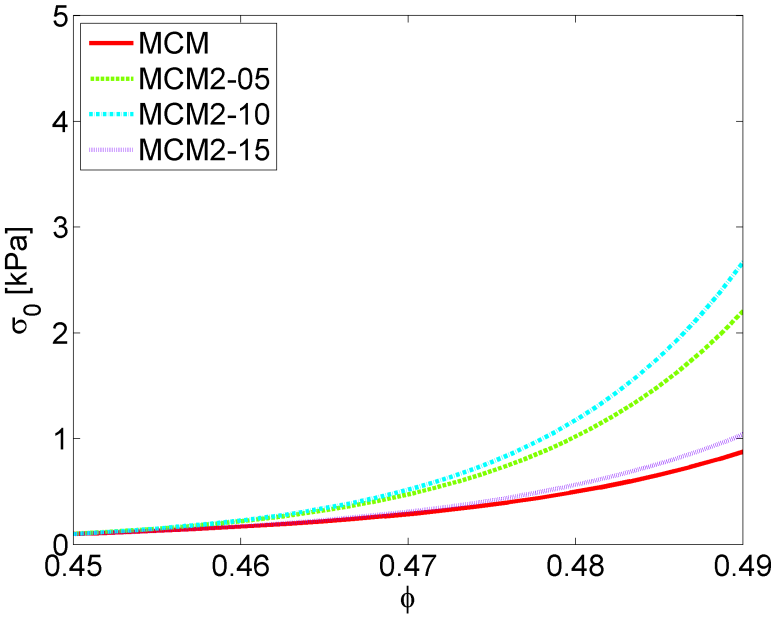

Figure 1.24: Compressive yield stress as a function of sediment volume fraction for Clay 2 at dosages of 0.5, 1.0 and 1.5% by mass of cement compared to the modified control mix

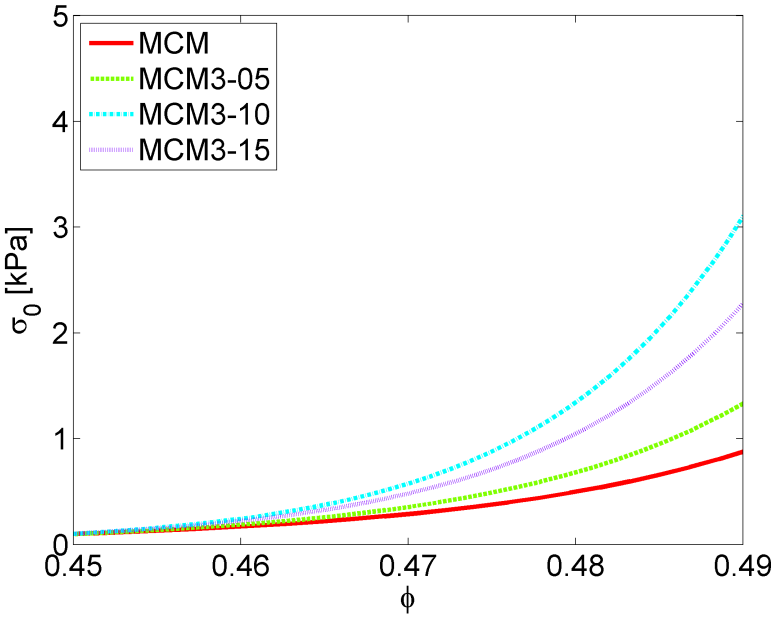

Figure 1.25: Compressive yield stress as a function of sediment volume fraction for Clay 3 at dosages of 0.5, 1.0 and 1.5% by mass of cement compared to the modified control mix

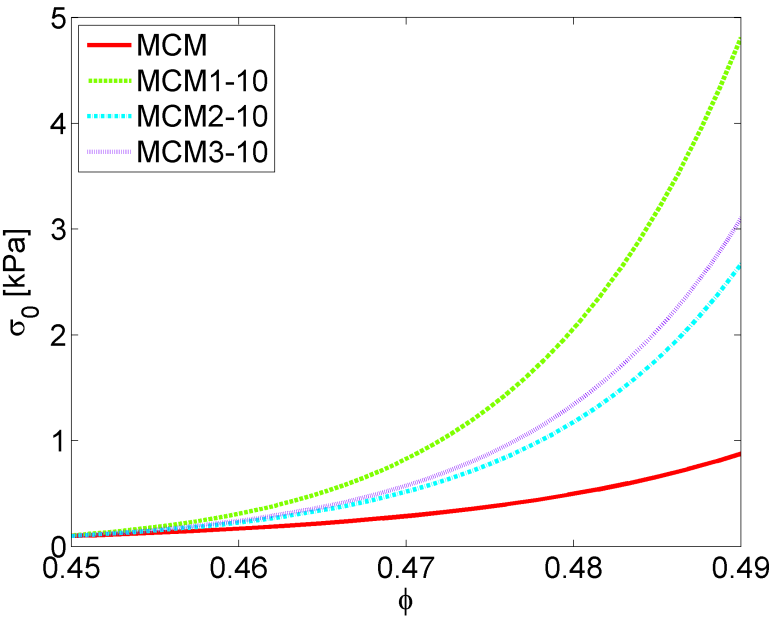

Figure 1.26: Compressive yield stress as a function of sediment volume fraction for all clays at a dosage of 1.0% by mass of cement compared to the modified control mix

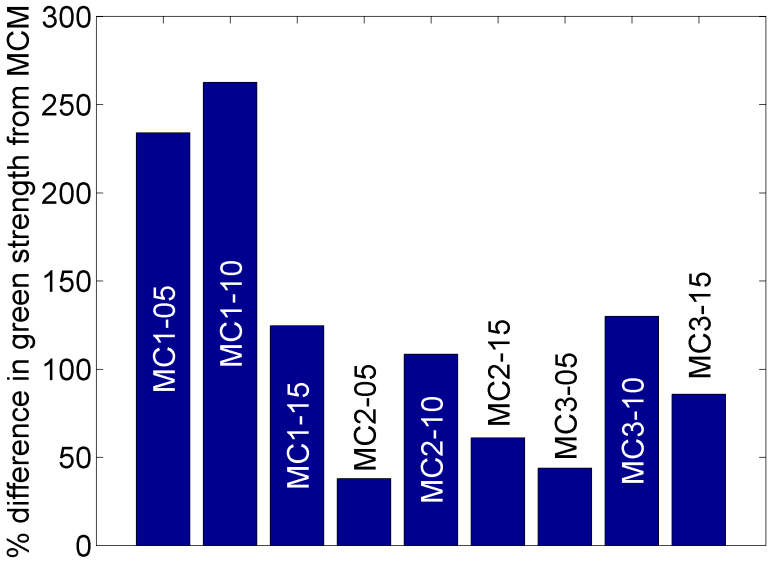

Figure 1.27: Effect of clay dosage on green strength results

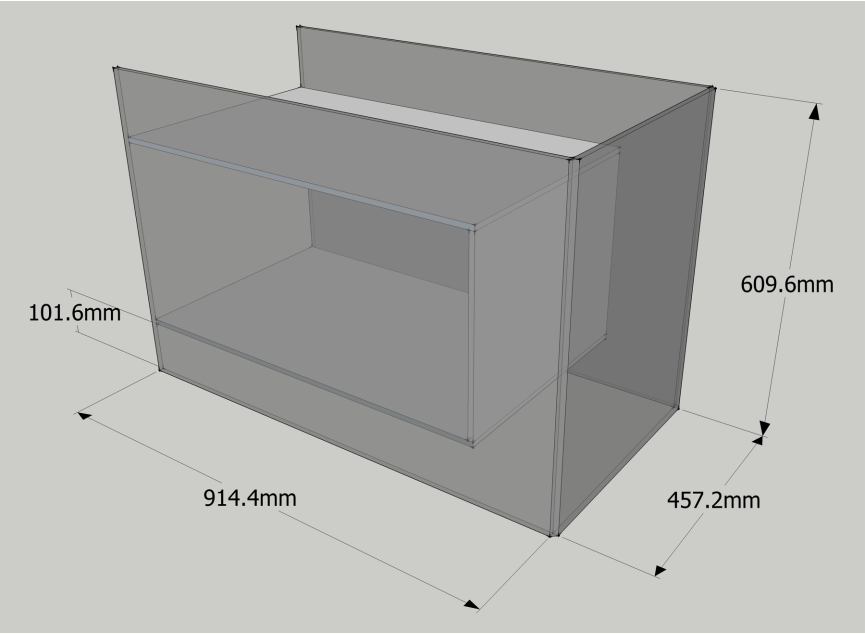

Figure 1.28: Minipaver developed at Iowa State University

slab stands free without any edge support. The slab has a cross section of 102 × 457 mm (4 × 18 in) and approximate length of 750 mm (30 in). The quality for the concrete slab is dependent on the consolidability of the concrete. This is determined by: a) how the concrete flows from the vertical shaft into the forming channel; b) how it consolidates under the static pressure exerted by the forming plate of the paver, and c) how it maintains the shape of the free-standing edges after the slipform process.

Results from the minipaver for MCM, MCM1-05, MCM1-10, MCM2-10 and MCM3-10 are shown in Figures 1.30 through 1.33. The images shown in these figures are a plan view of the slabs with the casting direction from the top of the page to the bottom of the page. From the plan views, the surface smoothness, which indicates proper consolidation, and edge stability, which indicates sufficient green strength, can be observed. In Figure 1.30, the MCM mix is shown. Without any clay, although the pavement surface is smooth, the edges are not parallel. Additionally, the surfaces near the edges are not smooth due to the excessive slump. Results for mixes containing 1.0% clay show improved edge straightness, while maintaining a degree of surface smoothness. However, for MCM1, the surface is much more rough compared to the other clay mixes (Figure 1.31). Using only 0.5% Clay 1 results in both superior smoothness and edge stability as shown in Figure 1.34.

In order to quantify shape stability, the edge slump ratio was measured. The edge slump is taken as the ratio between the height of the pavement at the centerline and the average height of the pavement at the outer edges. A ratio of 1 would indicate zero edge slump and high shape stability, while an edge slump ratio less than 1 would indicate less than ideal shape stability. The results of this test are given in Figure 1.35. These results along with the photos confirm that the composition with 0.5% Clay 1 produced the pavement with the smoothest surface and straightest edges. The results are also consistent with those obtained by Mbele for other SFSCC mixes [38].

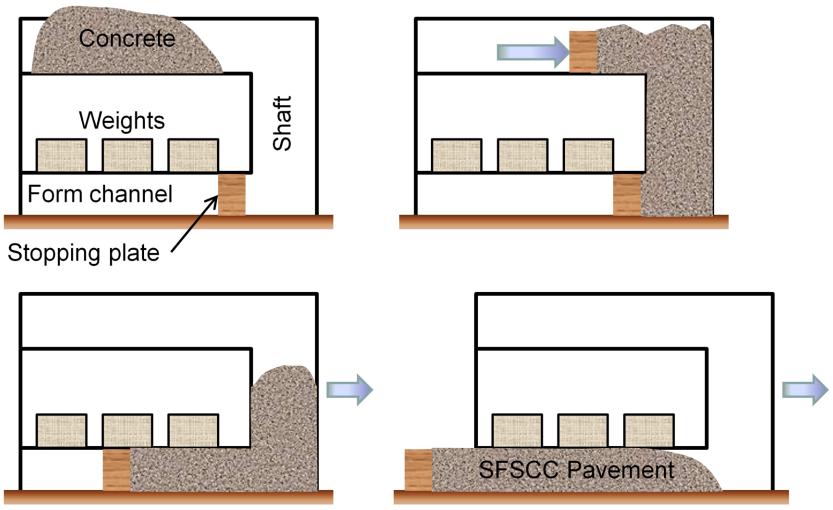

Figure 1.29: Schematic of minipaver process

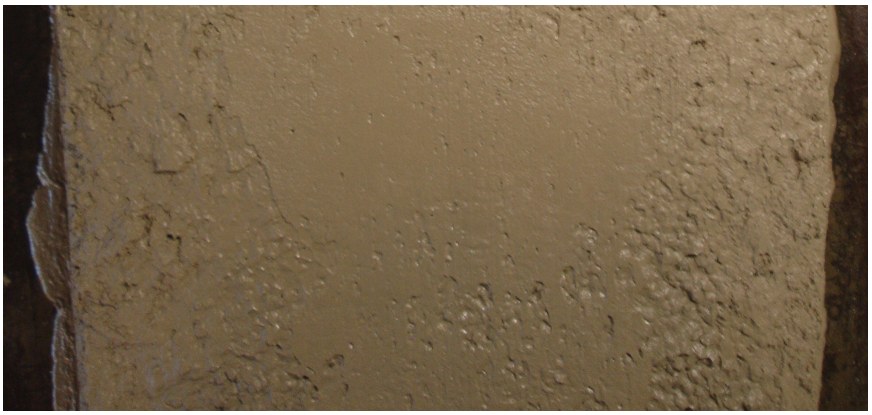

Figure 1.30: Plan view of MCM pavement from the minipaver

Figure 1.31: Plan view of MCM1-10 pavement from the minipaver

Figure 1.32: Plan view of MCM2-10 pavement from the minipaver

Figure 1.33: Plan view of MCM3-10 pavement from the minipaver

Figure 1.34: Plan view of MCM1-05 pavement from the minipaver

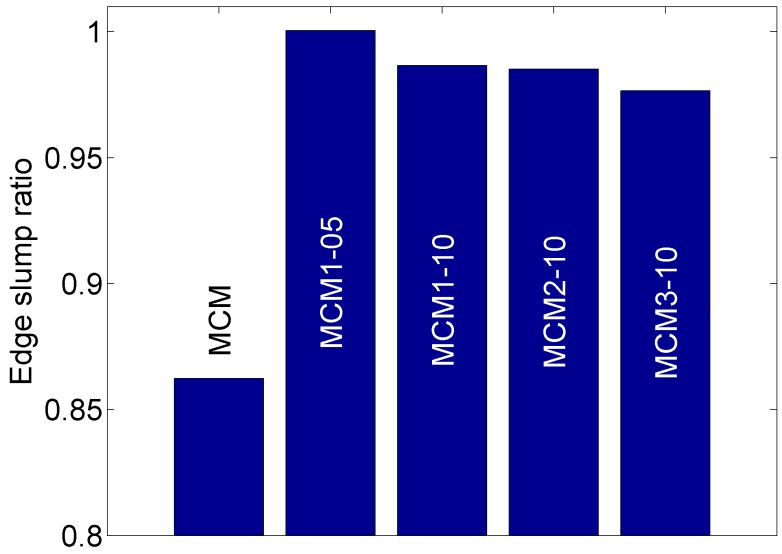

Figure 1.35: Edge slump for select SFSCC mixes tested with the minipaver

Summary

This investigation has shown a direct relationship between macro and micro behaviors (minipaver, green strength and compressive yield stress, respectively) which suggests the influence of flocculation strength on green strength. Optimal dosages of each clay were determined to be 1.0% by mass of cement with respect to both σ_0 and green strength. These optimal mixes showed improved green strength without sacrificing flowability during the minipaver test. Clay 1 showed the greatest increase in green strength and compressive yield stress and also showed the straightest edges during the minipaver test with only 0.5% by mass of cement. These results demonstrate that it is possible to design concrete to be both flowable and shape-stable and that clays at very small dosages can be beneficial in achieving this balance.

1.3 Further clay studies

In this section, additional investigations of clays are presented including the influence of clays on the particle packing of the dry system and shear oscillatory rheology.

1.3.1 Clay influences on particle packing

One possible explanation of how clays influence the green strength of cement and concrete is that the clay particles fill in the interstices of the microstructure, thereby increasing the packing fraction. Under compression, the stress can be distributed over more particles, leading to a stronger structure. In order to determine the packing fraction of the dry mix, a Compressive Packing Model (CPM) developed by De Larrard [72] was used. This model is based on the Apollonian model, where smaller particles fit in the interstices of larger ones. Considering a set of n granular sizes with a diameter of d_i, where $d_1 \geq d_2 \geq ... \geq d_n$. The *virtual* packing fraction, γ_i, represents the maximum packing fraction achievable for a diameter, d_i, as a result of infinite compaction energy and is given by Equation 1.10 [72]:

$$\gamma_i = \frac{\beta_i}{1 - \sum_{j=1}^{i-1}[1 - \beta_i + b_{ij}\beta_i(1 - 1/\beta_i)]y_j - \sum_{j=i+1}^{n}[1 - a_{ij}\beta_i/\beta_j]y_j}, \tag{1.10}$$

where β_i is the specific packing fraction of a class i, b_{ij} is the wall effect exerted by class j on class i, a_{ij} is the loosening effect exerted by class j on class i, and y_i is the volume content of class i in proportion to the total volume. Both the loosening effect and wall effect can be determined experimentally, and de Larrard gives the following relationships [72].

$$a_{ij} = \sqrt{1 - (1 - d_j/d_i)^{1.02}} \tag{1.11}$$

$$b_{ij} = 1 - (1 - d_j/d_i)^{1.5} \tag{1.12}$$

In order to obtain the *actual* packing fraction, since an infinite compaction energy is not realistic, Equation 1.13 is used to adjust the virtual packing [72]:

$$K = \sum_{i=1}^{n} \frac{y_i/\beta_i}{1/\Phi - 1/\gamma_i}, \tag{1.13}$$

where K is the compaction index and Φ is the solid content of the concrete. The compaction index depends on the degree of compaction and has been experimentally correlated to different compaction techniques such as rodding, vibration and vibration with compression. Values are given in Table 1.11

Table 1.11: Compaction indices (K values) for different compaction techniques [72]

Pouring [74]	Rodding [75]	Vibration [76]	Vibration and compression [77]
4.1	4.5	4.75	9

Table 1.12: Packing fractions for mixes containing either fly ash or one of three clays

Dry materials	Packing fraction	% difference from cement
Cement	0.80371	-
Cement + FA	0.80736	0.4541
Cement + Clay 1	0.80488	0.1456
Cement + Clay 2	0.80356	-0.0187
Cement + Clay 3	0.80420	0.0610

[72]. Using this model, de Larrard et al. have been able to improve not only compressive strengths, but also flowability and segregation [73].

The CPM was employed to determine the influence of clays on the packing fraction. Dry materials from all of the mixes tested using the compressive rheology method were analyzed using a compaction index of 9 corresponding to vibration and compression. The results for dry mixes with a single admixture (fly ash or one of three clays) are shown in Table 1.12 while the results for dry mixes containing fly ash and one of three clays are shown in 1.13. The results show that although differences can be seen between the packing fractions, they are all below half a percent as compared to the control mix. These results confirm that the clays do not influence the packing density enough to consider an altered packing fraction as the reason for the increase in the green strength.

1.3.2 Clay influences on shear oscillatory rheology

Previously in this chapter, rheological methods have been employed to study the effects of varying stress on the fresh state structure of cement pastes. In this particular section, an oscillatory shear method is used in order to understand how the structure gains strength over time. This method

Table 1.13: Packing fractions for mixes containing either fly ash and one of three clays

Dry materials	Packing fraction	% difference from cement
Cement + FA	0.80736	-
Cement + FA + 0.5% Clay 1	0.80782	0.0570
Cement + FA + 1.0% Clay 1	0.80829	0.1152
Cement + FA + 1.5% Clay 1	0.80875	0.1722
Cement + FA + 0.5% Clay 2	0.80725	-0.0136
Cement + FA + 1.0% Clay 2	0.80712	-0.0296
Cement + FA + 1.5% Clay 2	0.80702	-0.0421
Cement + FA + 0.5% Clay 3	0.80760	0.0297
Cement + FA + 1.0% Clay 3	0.80765	0.0359
Cement + FA + 1.5% Clay 3	0.80778	0.0520

involves applying an sinusoidal strain and measuring the resulting stress as outlined in Equations 1.14 and 1.15. Applied strains are small enough not to destroy the structure; this region is called the linear viscoelastic domain (LVD). Figure 1.36 demonstrates responses of an ideal liquid and solid to an oscillatory strain within the LVD. The phase angle, δ, is the time difference between the applied strain the stress response. For ideal liquids, the phase angle is 90°, indicating a pure viscous response, while for ideal solids, the phase angle is 0°, indicating a pure elastic response. As cement gains strength, the phase angle will decrease from 90° to 0° once it is hardened.

$$\gamma = \gamma_a \cos(\omega t), \tag{1.14}$$

$$\tau = \tau_a \cos(\omega t + \delta), \tag{1.15}$$

In Equations 1.14 and 1.15, γ is the applied strain, γ_a is the strain amplitude, ω is the angular speed, t is time, τ is the stress response and τ_a is the stress amplitude. The ratio between the stress and strain is the complex modulus, G^*, and is composed of two components: an elastic part, which is called the storage modulus, G', and the viscous part, which is called the loss modulus, G''. These relations are given in Equations 1.16, 1.17 and 1.18:

$$G* = \frac{\tau}{\gamma} = G' + \imath G'', \tag{1.16}$$

$$G' = \frac{\tau_a}{\gamma_a} \cos\delta, \tag{1.17}$$

$$G'' = \frac{\tau_a}{\gamma_a} \sin\delta, \tag{1.18}$$

where $\imath$ is $\sqrt{-1}$. Fluid-like behavior is indicated by $G'' \gg G'$ while solid-like behavior is indicted for $G' \gg G''$. This method has been used for cement successfully in a number of studies [78, 79, 80, 81].

In order to ensure that measurements are taken within the LVD, a critical strain and critical frequency must be satisfied. These values are determined by strain and frequency sweeps respectively. During a strain sweep, the frequency is held constant while the strain is increased over time. The LVD boundary is characterized by a drop in G^*; before the critical strain, G^* remains constant. During a frequency sweep, the strain is held constant while the frequency is increased. Similarly, the critical frequency is marked by the decrease in G^*.

Mix compositions and methods

Four paste compositions were used in this study: a control mix, CM and three mixes containing 1% clay by mass, CM1, CM2 and CM3; the same mix proportions given previously in Table 1.4. All mixes have a solids volume fraction of 0.45 and a w/b of 0.39. After mixing according to the same protocol as Table 1.6, each composition was subjected to a series of strain and frequency sweeps in order to determine the critical strain and frequency values. A new batch was used for both the strain and frequency sweeps. For the strain sweeps, the strain was increased from 0.0001 to 1 while the frequency was held constant at 1 Hz. For the frequency sweeps, the frequency was increased from 0.1 to 10 Hz while the strain was held constant at 0.0001. After the strain and frequency sweeps, time sweeps were performed on each composition at a strain of 0.0001 and frequencies of 0.1, 0.5, 1, 2, 4, and 8 Hz for 1500 s. Each strain and frequency used was within the LVD. An example of the time sweep is shown in Figure 1.37. Both the complex modulus and phase lag evolution are shown. As time progresses, the cement paste stiffens indicated by the increase in G^* and the decrease of δ. For the cement pastes studied, δ typically decreased from 80° to 15°.

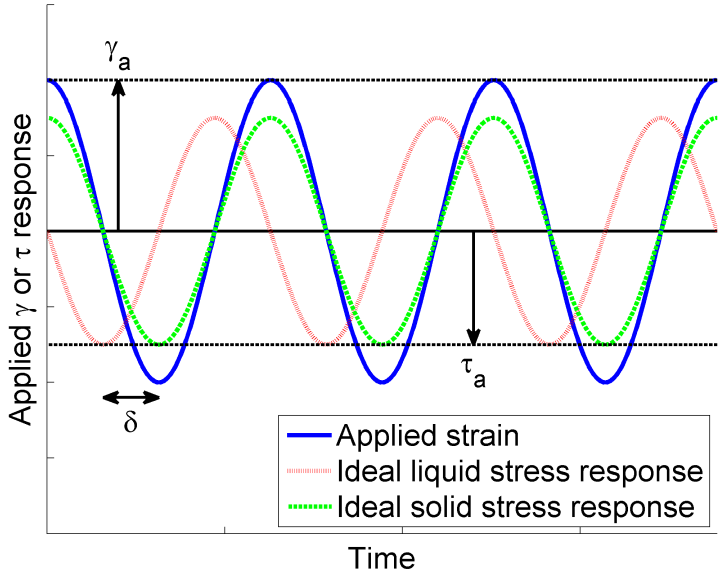

Figure 1.36: Shear responses of ideal liquid and solids under applied oscillatory strain

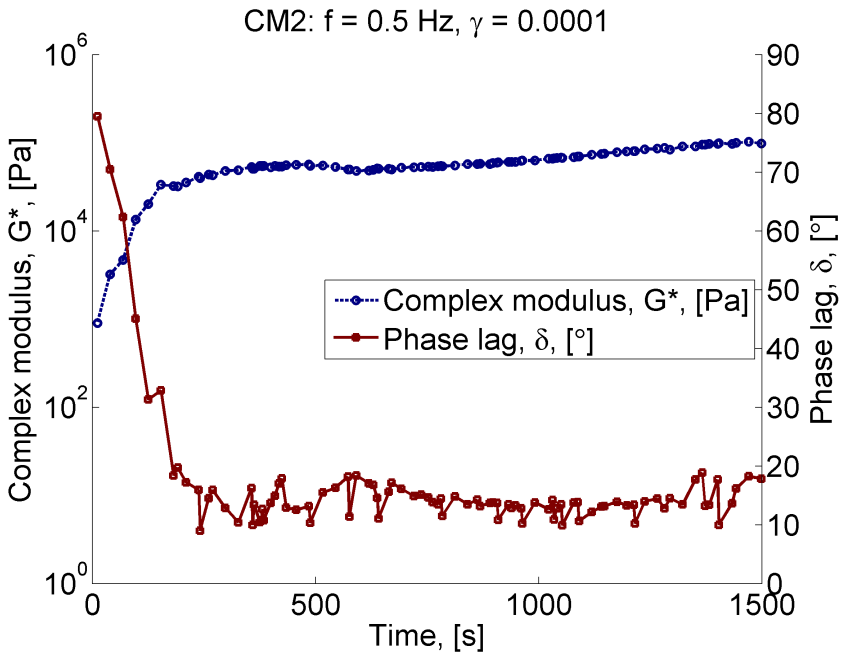

Figure 1.37: Complex modulus and phase lag evolution over time for an applied oscillatory strain of 0.0001 with a frequency of 0.5 Hz

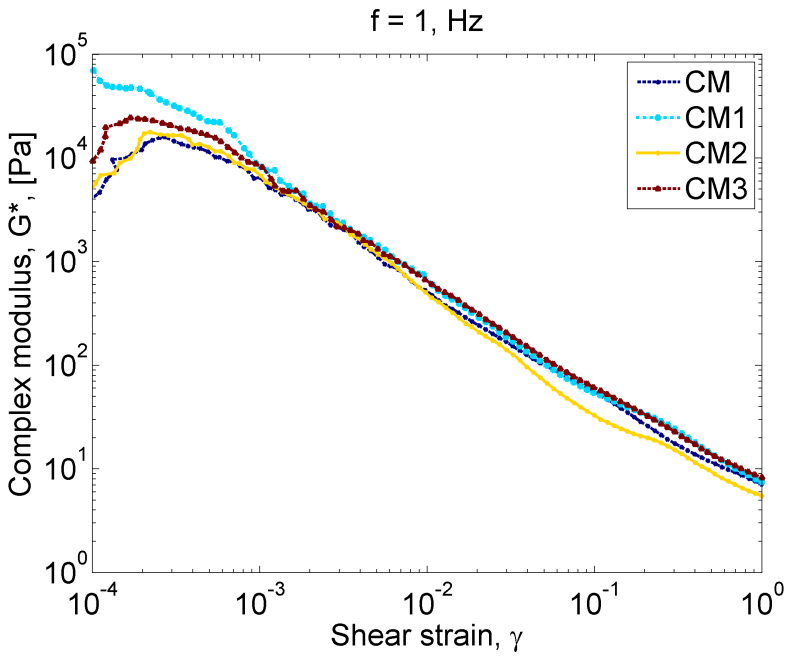

Figure 1.38: Complex modulus responses to a strain sweep from 0.0001 to 1 with a frequency of 1 Hz for the CM and CM1-3

Shear oscillatory rheology results and discussion

Figures 1.38 and 1.39 present the strain and frequency sweep results for all four mixes. For the strain sweep, all mixes begin to decrease around a strain of 0.0002. After which, the complex modulus begins to decrease. Similarly, for the frequency sweep, all mixes begin to decrease around a frequency of 11 Hz. As a result, for the time sweeps, the strain rate was held constant at 0.0001 while the frequency was varied from 0.1 to 10 Hz.

The evolution of the complex modulus for varying frequencies for each material is given in Figures 1.40 through 1.43. Over time, G^* increases, indicating that the mixes are stiffening. In general, higher frequencies have higher rates of stiffening, although there seems to be no correlation between frequency and final $G*$. Higher frequencies may induce more collisions between particles, leading to faster flocculation. Figures 1.44 and 1.45 compare all the materials at frequencies of 0.1 and 8 Hz respectively concerning the evolution of the complex modulus. For a frequency of 0.1, it can be seen that the clay mixes all increase in G^* faster and to a higher level than the CM, indicating faster flocculation due to the clays. For a frequency of 8 Hz, the same phenomenon is seen.

In Figures 1.46 through 1.49, the evolution of the phase lag is shown for each material for varying frequencies. The results match the complex modulus evolution results in that the phase lag tends to decrease much more rapidly for higher frequencies indicating a transition from a liquid-state to a solid-state. Figures 1.50 and 1.51 compare all the materials at frequencies of 0.1 and 8 Hz respectively for the evolution of the phase lag. Again, the clays all achieve a lower phase lag quicker than CM. As before, this indicates a faster flocculation due to the clays.

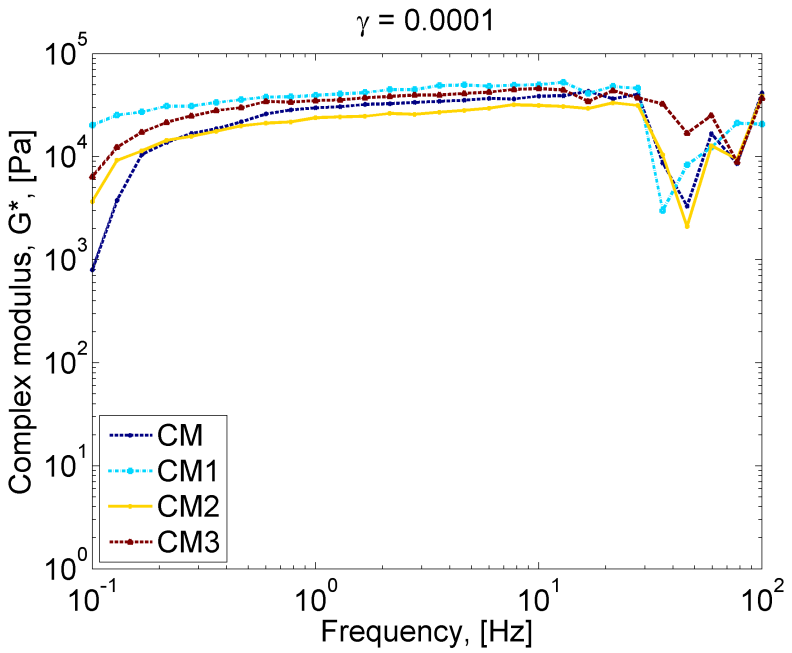

Figure 1.39: Complex modulus responses to a frequency sweep from 0.1 to 10 for a strain of 0.0001 for the CM and CM1-3

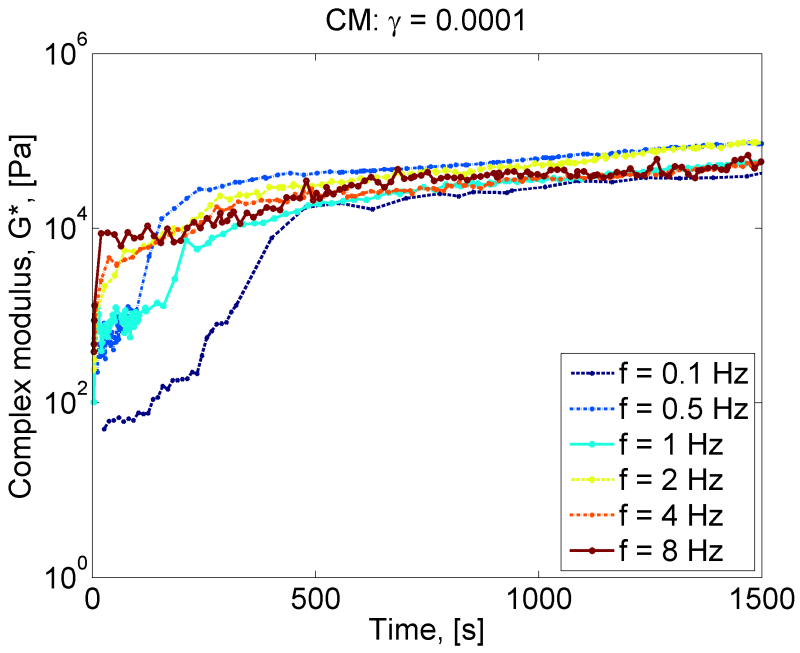

Figure 1.40: Complex modulus evolution for a strain of 0.0001 and frequencies of 0.1, 0.5, 1, 2, 4, and 8 Hz for the CM

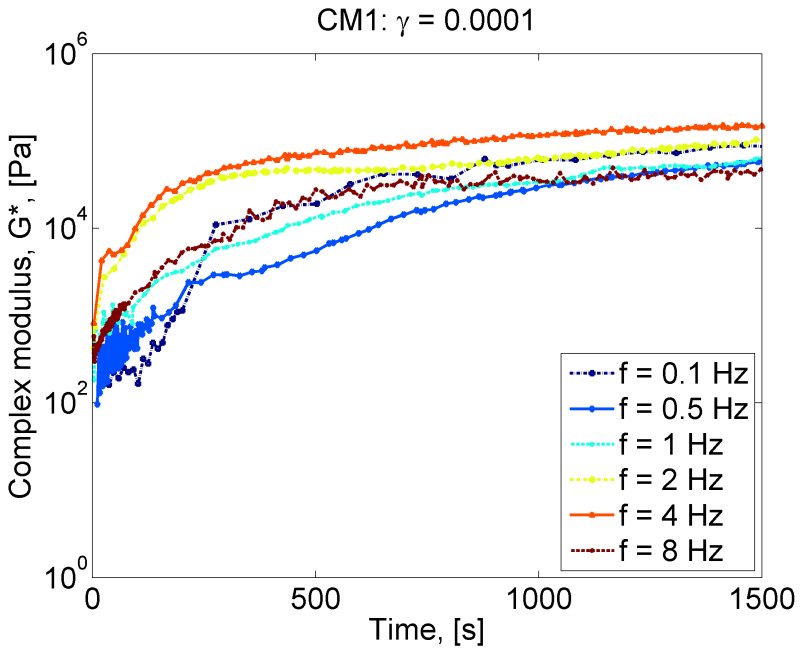

Figure 1.41: Complex modulus evolution for a strain of 0.0001 and frequencies of 0.1, 0.5, 1, 2, 4, and 8 Hz for the CM1

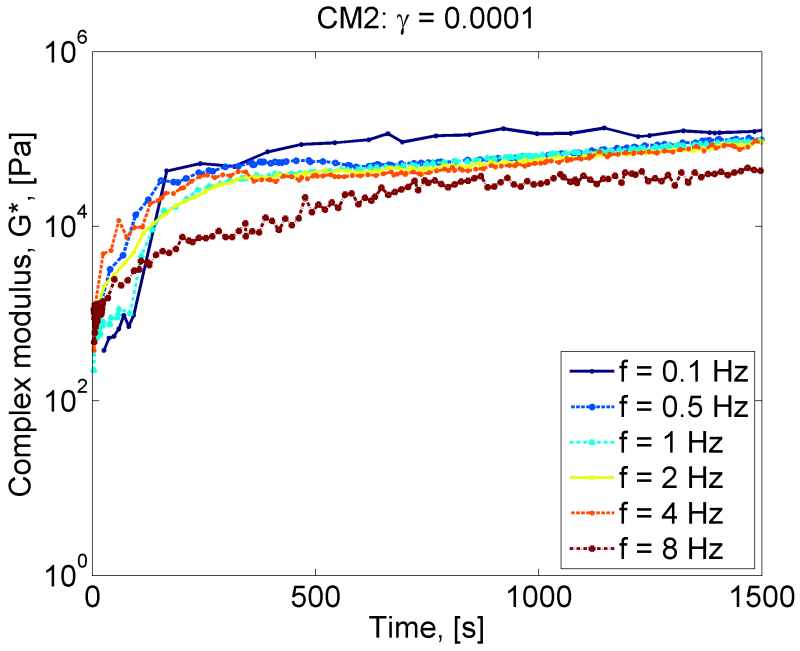

Figure 1.42: Complex modulus evolution for a strain of 0.0001 and frequencies of 0.1, 0.5, 1, 2, 4, and 8 Hz for the CM2

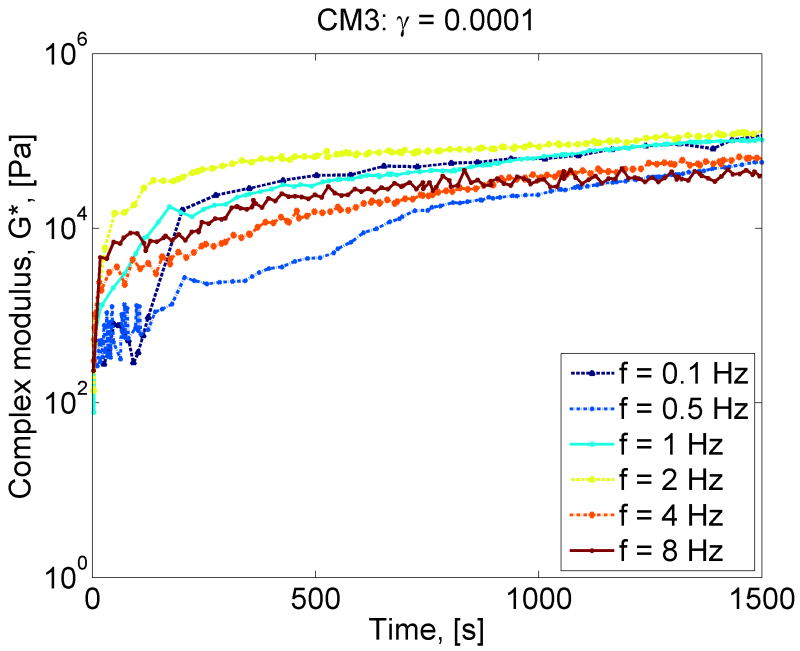

Figure 1.43: Complex modulus evolution for a strain of 0.0001 and frequencies of 0.1, 0.5, 1, 2, 4, and 8 Hz for the CM3

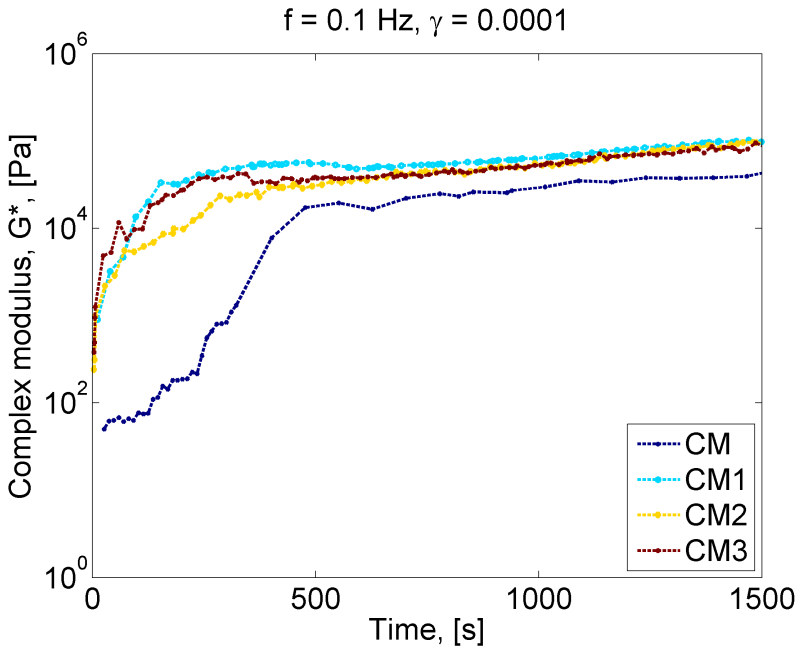

Figure 1.44: Complex modulus evolution for a strain of 0.0001 and frequency of 0.1 Hz for the CM and CM1-3

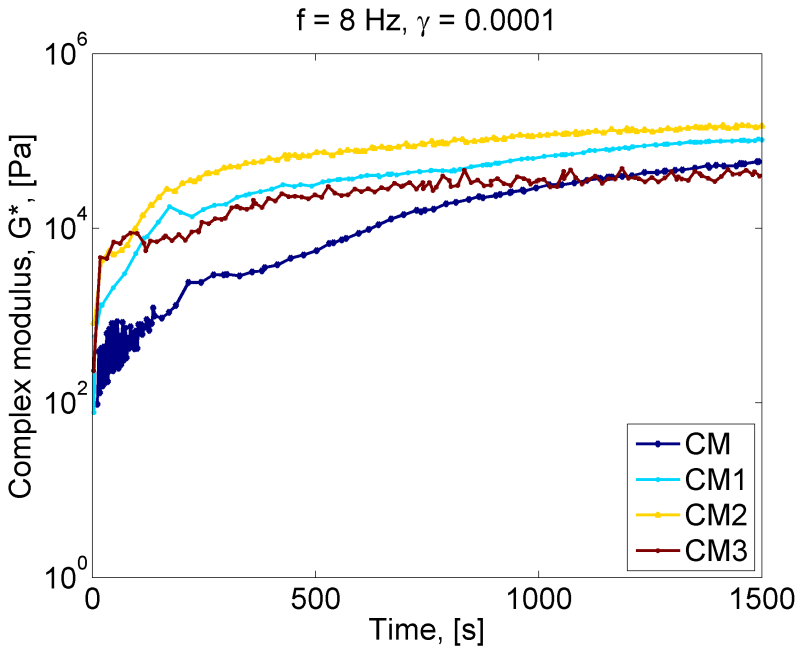

Figure 1.45: Complex modulus evolution for a strain of 0.0001 and frequency of 8 Hz for the CM and CM1-3

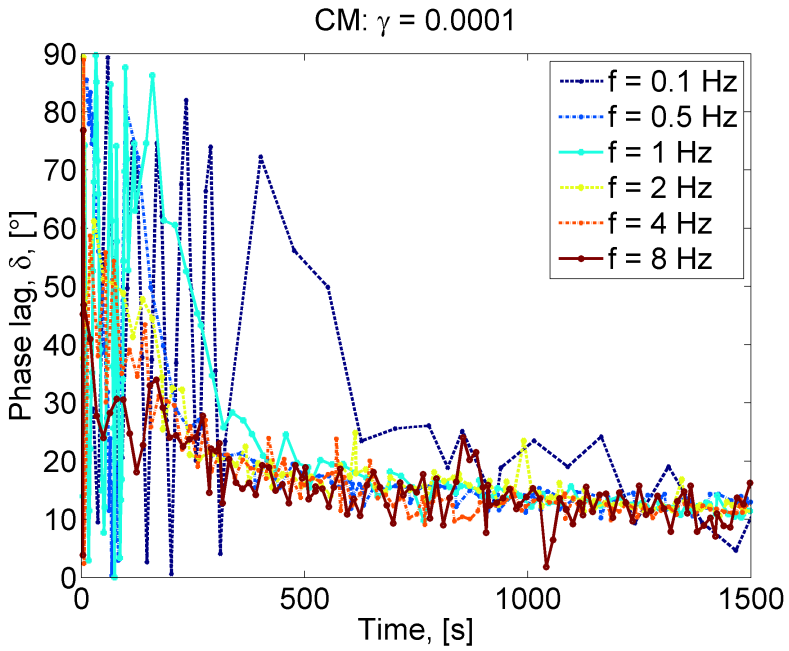

Figure 1.46: Phase lag evolution for a strain of 0.0001 and frequencies of 0.1, 0.5, 1, 2, 4, and 8 Hz for the CM

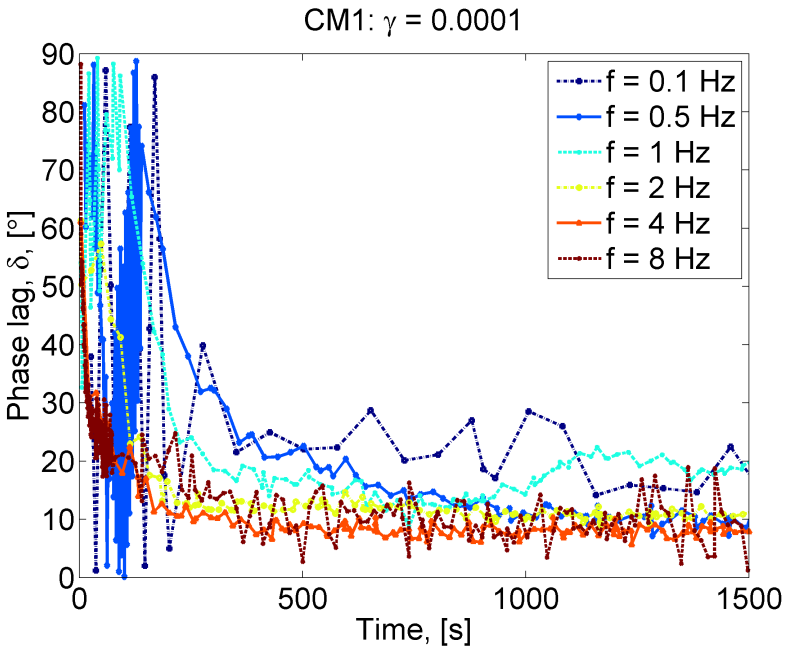

Figure 1.47: Phase lag evolution for a strain of 0.0001 and frequencies of 0.1, 0.5, 1, 2, 4, and 8 Hz for the CM1

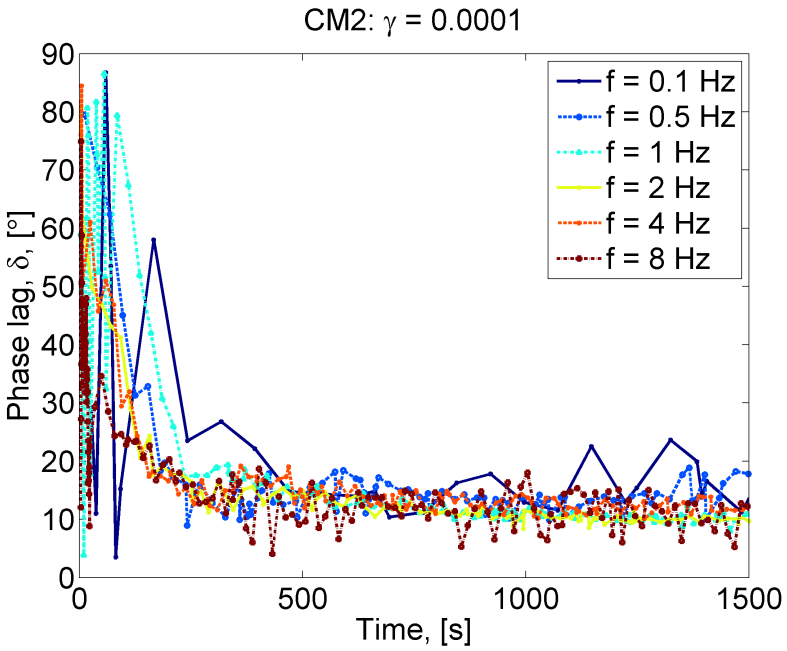

Figure 1.48: Phase lag evolution for a strain of 0.0001 and frequencies of 0.1, 0.5, 1, 2, 4, and 8 Hz for the CM2

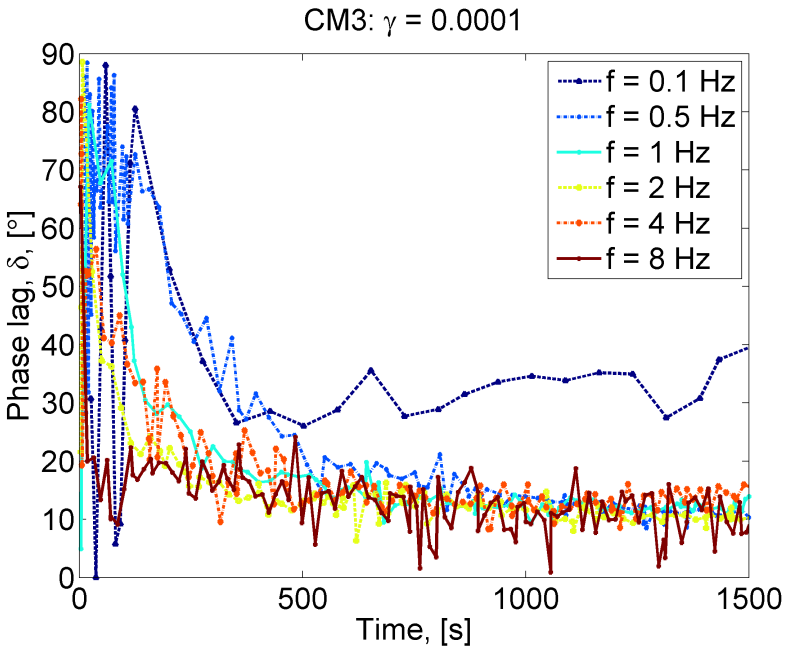

Figure 1.49: Phase lag evolution for a strain of 0.0001 and frequencies of 0.1, 0.5, 1, 2, 4, and 8 Hz for the CM3

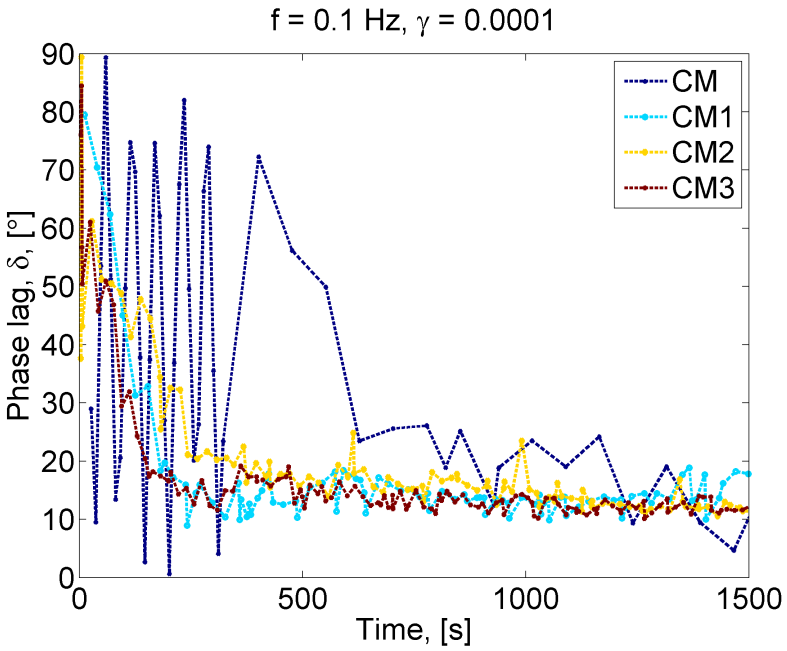

Figure 1.50: Phase lag evolution for a strain of 0.0001 and frequency of 0.1 Hz for the CM and CM1-3

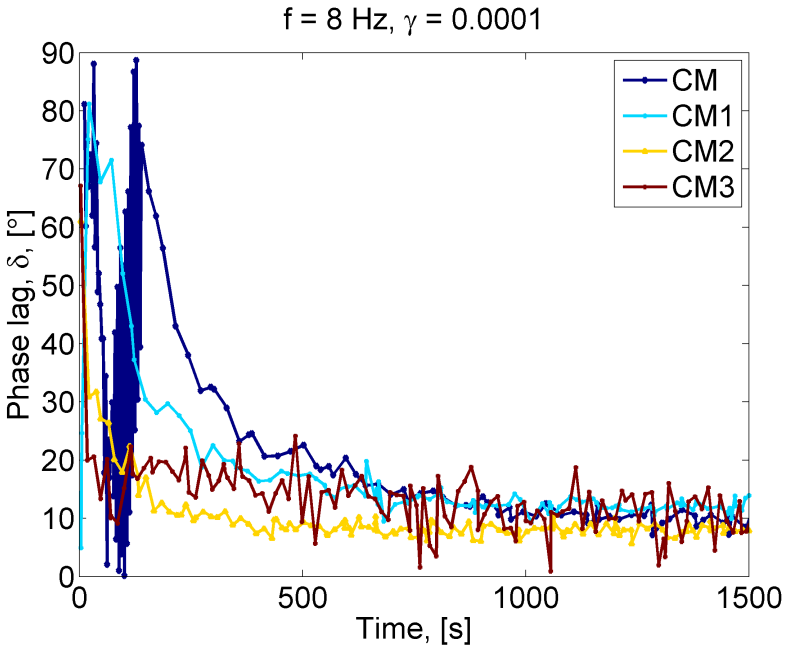

Figure 1.51: Phase lag evolution for a strain of 0.0001 and frequency of 8 Hz for the CM and CM1-3

Shear oscillatory rheology summary

In this section, clays were shown to increase the rate of stiffening from an oscillatory method perspective. Over time, clays increased the rate of gain as well as the magnitude of the complex modulus. Also, the phase lag was shown to decrease faster for clay mixes and also showed a smaller final angle. Future work at Northwestern University will attempt to correlate these oscillatory rheology results to oscillatory methods with higher frequencies such as ultrasonic methods currently investigated by Dr. Jae Hong Kim [82].

Bibliography

[1] Kejin Wang, Surendra Shah, David White, Joseph Gray, Thomas Voigt, Lu Gang, Jiong Hu, Clinton Halverson, and Bekir Pekmezci. Self-consolidating concrete applications for slip-form paving: Phase I (feasibility study). Final Report TPF-5(098), Center for Portland Cement Concrete Pavement Technology, 2005.

[2] Katherine Kuder. *Extruded Fiber-Reinforced Cementitious Composites for Use in Residential Construction*. PhD thesis, Northwestern University, Evanston, IL, December 2005.

[3] Katherine Kuder and Surendra Shah. Rheology of extruded cement-based materials. *ACI Materials Journal*, 104(3):283–290, 2007.

[4] Thomas Voigt, Tim Malonn, and Surendra Shah. Green and early age compressive strength of extruded cement mortar monitored with compression tests and ultrasonic techniques. *Cement and Concrete Research*, 36(5):858–867, 2006.

[5] Zied Soua, Oliver Larue, Eugène Vorobiev, and Jean-Louis Lanoisellé. Estimation of floc size in highly concentrated calcium carbonate suspension obtained by filtration with dispersant. *Colloids and Surfaces A*, 274(1-3):1–10, 2006.

[6] Richard Buscall and Lee White. The consolidation of concentrated suspensions, part 1. - the theory of sedimentation. *Journal of Chemical Societies Faraday Transactions*, 83(3):873–891, 1987.

[7] Nathan Tregger, Margaret Pakula, and Surendra Shah. Influence of clays on the rheology of cement pastes. *Cement and Concrete Research*, 40(3):384–391, 2010.

[8] Peter Jarvis, Bruce Jefferson, John Gregory, and Simon Parsons. A review of floc strength and breakage. *Water Research*, 39(14):3121–3137, 2005.

[9] Dean-Mo Liu. Theoretical determination of floc size in highly-concentrated zirconiawax suspensions. *Acta Materialia*, 50(8):1927–1935, 2002.

[10] Dean-Mo Liu. Particle packing and rheological property of highly-concentrated ceramic suspensions: ϕ determination and viscosity prediction. *Journal of Materials Science*, 35(21):5503–5507, 2000.

[11] Leslie Struble and Guo-Kuang Sun. Viscosity of portland cement paste as a function of concentration. *Advanced Cement Based Materials*, 2(2):62–69, 1995.

[12] C Wildemuth and M Williams. Viscosity of suspensions modeled with a shear-dependent maximum packing fraction. *Rheologica Acta*, 23(6):627–635, 1984.

[13] James Zhou, Tunan Fang, Guihua Luo, and Peter Uhlherr. Yield stress and maximum packing fraction of concentrated suspensions. *Rheologica Acta*, 34(6), 1995.

[14] Sandrine Mansoutre, Pierre Colombet, and H. van Damme. Water retention and granular rheological behavior of fresh C_3S paste as a function of concentration. *Cement and Concrete Research*, 29(9):1441–1453, 1999.

[15] D Thomas, Simon Judd, and Nick Fawcett. Flocculation modeling: a review. *Water Research*, 33(7):1572–1592, 1999.

[16] Stephen Johnson, George Franks, Peter Scales, David Boger, and Thomas Healy. Surface chemistry-rheology relationships in concentrated mineral suspensions. *International Journal of Mineral Processing*, 58(1-4):267–304, 2000.

[17] Geoffrey Tattersall and Phil Banfill. *The Rheology of Fresh Concrete*. Pitman Publishing Inc., Marshfield, MA, 1983.

[18] Richard Shaughnessy and Peter Clark. The rheological behavior of fresh cement pastes. *Cement and Concrete Research*, 18(3):327–341, 1988.

[19] Howard Barnes. Thixotropy - A review. *Journal of Non-Newtonian Fluid Mechanics*, 70(1-2):1–33, 1997.

[20] David Williams, Aaron Saak, and Hamlin Jennings. Influence of mixing on the rheology of fresh cement paste. *Cement and Concrete Research*, 29(9):1491–1496, 1999.

[21] Joseph Assaad, Kamal Khayat, and Habib Mesbah. Assessment of thixotropy of flowable and self-consolidating concrete. *ACI Materials Journal*, 100(2):99–107, 2003.

[22] Nicolas Roussel. Steady and transient flow behaviour of fresh cement pastes. *Cement and Concrete Research*, 35(9):1656–1664, 2005.

[23] Raissa Ferron, Amedeo Gregori, Zhihui Sun, and Surendra Shah. Rheological method to evaluate structural buildup in self-consolidating concrete cement pastes. *ACI Materials Journal*, 104(3):242–250, 2007.

[24] Sebastien Jarny, Nicolas Roussel, Robert Le Roy, and Philippe Coussot. Modelling thixotropic behavior of fresh cement pastes from mri measurements. *Cement and Concrete Research*, 38(5):616–623, 2008.

[25] Jon Wallevik. Rheological properties of cement paste: thixotropic behavior and structural breakdown. *Cement and Concrete Research*, 39(1):14–29, 2009.

[26] Peter Billberg. *Form Pressure Generated by Self-Compacting Contrete - Influence of Thixotropy and Structural Behaviour at Rest*. PhD thesis, Royal Institute of Technology, Stockholm, Sweden, September 2006.

[27] Raissa Ferron. *Formwork Pressure of Self-Consolidating Concrete: Influence of Flocculation Mechanisms, Structural Rebuilding, Thixotropy and Rheology*. PhD thesis, Northwestern University, Evanston, IL, December 2008.

[28] Joseph Assaad, Kamal Khayat, and Habib Mesbah. Variation of formwork pressure with thixotropy of self-consolidating concrete. *ACI Materials Journal*, 100(1):29–37, 2003.

[29] Nicolas Roussel. A thixotropy model for fresh fluid concretes: theory, validation and applications. *Cement and Concrete Research*, 36(10):1797–1806, 2006.

[30] Jean Tchamba, Sofiane Amziane, Guillaume Ovarlez, and Nicolas Roussel. Lateral stress exerted by fresh cement paste on formwork: laboratory experiments. *Cement and Concrete Research*, 38(4):459–466, 2008.

[31] R Buscall. The elastic properties of structured dispersions: a simple centrifuge method of examination. *Colloids and Surfaces*, 5(4):269–283, 1982.

[32] Irvin Krieger and Thomas Dougherty. A mechanism for non-Newtonian flow in suspensions of rigid spheres. *Journal of Rheology*, 3(1):137–152, 1959.

[33] Robin Ball and Peter Richmond. Dynamics of colloidal dispersions. *Physics and Chemistry of Liquids*, 9(2):99–116, 1980.

[34] Hans Wyss, Elena Tervoort, and Ludwig Gauckler. Mechanics and microstructures of concentrated particle gels. *Journal of the American Ceramics Society*, 88(9):2337–2348, 2005.

[35] Matthew Green, Maria Eberl, and Kerry Landman. Compressive yield stress of flocculated suspensions: determination via experiment. *American Institute of Chemical Engineering Journal*, 42(8):2308–2318, 1996.

[36] Kelly Miller, Wei Shi, Leslie Struble, and Charles Zukoski. Compressive yield stress of cement paste. In Sidney Diamond, Sidney Mindess, F Glasser, Lawrence Roberts, Jan Skalny, and Lillian Wakeley, editors, *Microstructrure of Cement-Based Systems/Bonding and Interfaces in Cementitious Materials*, pages 285–291, GET IT, GET IT 1995. Materials Research Society, GET IT.

[37] Research and Technology Center. Sem micrographs and elemental analyses of clays: Acti-gel, metamax and concresol. Materials Analysis Laboratory Log 06-180, USG Corporation, Libertyville, IL, 2006.

[38] Jean-Juste Mbele. Optimization of self-consolidating concrete for slip-form pavement. Master's thesis, Northwestern University, Evanston, IL, April 2006.

[39] LLC Active Minerals International. What is acti-gel ® 208 and how is it made? Product description, Active Minerals International, LLC, Hunt Valley, MD, 2007.

[40] Stephan Schmidt Gruppe. Concresol ® 105. Technical data sheet, Stephan Schmidt Gruppe, Dornburg, Germany, 2004.

[41] BASF Catalysts LLC. MetaMax ® PA high-reactivity metakaolin for pool plasters. Technical data sheet, BASF Corporation, Florham Park, NJ, 2007.

[42] Rafat Siddique and Juvas Klaus. Influence of metakaolin on the properties of mortar and concrete: A review. *Applied Clay Science*, 43(3-4):392–400, 2009.

[43] Efstratios Badogiannis and Sotiris Tsivilis. Exploitation of poor Greek kaolins: Durability of metakaolin concrete. *Cement and Concrete Composites*, 31(2):128–133, 2009.

[44] Efstratios Badogiannis, G Kakali, G Dimopoulou, Emmanuel Chaniotakis, and Sotiris Tsivilis. Metakaolin as a main cement constituent: Exploitation of poor Greek kaolins. *Cement and Concrete Composites*, 27(2):197–203, 2005.

[45] Efstratios Badogiannis, Vagelis Papadakis, Emmanuel Chaniotakis, and Sotiris Tsivilis. Exploitation of poor Greek kaolins: Strength development of metakaolin concrete and evaluation by means of k-value. *Cement and Concrete Research*, 34(6):1035–1041, 2004.

[46] Chi-Sun Poon, Liza Lam, Shi Kou, Yuk-Lung Wong, and Ron Wong. Rate of pozzolanic reaction of metakaolin in high-performance cement pastes. *Cement and Concrete Research*, 31(9):1301–1306, 2001.

[47] Stanley Wild, Jamal Khatib, and Alan Jones. Relative strength, pozzolanic activity and cement hydration in superplasticised metakaolin concrete. *Cement and Concrete Research*, 26(10):1537–1544, 1996.

[48] P Bredy, Michel Chabannet, and Jean Pera. Microstructural and porosity of metakaolin blended cements. In *Materials Research Society Symposium*, volume 137, pages 431–436, 1989.

[49] Grace Construction Products. Daracem ® 19 high-range water-reducing admixture. Product description DC-8I, W. R. Grace & Company, Cambridge, MA, 2007.

[50] Research and Technology Center. Sympatec particle size analyzer-laser diffraction technique for cement. Materials Analysis Laboratory Log 06-170, USG Corporation, Libertyville, IL, 2006.

[51] Alpena Plant. Cement mill test report. Mill test report, Lafarge North America, Alpena, MI, December 2006.

[52] Oak Creek. Fly ash analysis. Properties report, Lafarge North America, Lock Port, IL, July 2006.

[53] Research and Technology Center. Sympatec particle size analyzer-laser diffraction technique for fly ash class C. Materials Analysis Laboratory Log 06-170, USG Corporation, Libertyville, IL, 2006.

[54] BASF Catalysts LLC. Chemical and physical characteristics of Metamax ® HRM. Product description, BASF Corporation, Florham Park, NJ, 2007.

[55] Research and Technology Center. Sympatec particle size analyzer-laser diffraction technique for Acti-Gel. Materials Analysis Laboratory Log 06-170, USG Corporation, Libertyville, IL, 2006.

[56] Research and Technology Center. Sympatec particle size analyzer-laser diffraction technique for Concresol. Materials Analysis Laboratory Log 06-170, USG Corporation, Libertyville, IL, 2006.

[57] Research and Technology Center. Sympatec particle size analyzer-laser diffraction technique for MetaMax. Materials Analysis Laboratory Log 06-170, USG Corporation, Libertyville, IL, 2006.

[58] Tasos Papanastasiou. Flow of materials with yield. *Journal of Rheology*, 31(5):385–404, 1987.

[59] P Mills, J Goodwin, and B Grover. Shear field modification of strongly flocculated suspensions - aggregate morphology. *Colloid Polymer Science*, 269(9):949–963, 1991.

[60] P Andersen. The effect of superplasticizers and air-entraining agents on the zeta potential of cement particles. *Cement and Concrete Research*, 16(6):931–940, 1986.

[61] Jennifer Lewis, Hiro Matsuyama, Glen Kirby, Sherry Morissette, and Francis Young. Polyelectrolyte effects on the rheological properties of concentrated cement suspensions. *Journal of the American Ceramics Society*, 83(8):1905–1913, 2000.

[62] Ane Kjeldsen, Robert Flatt, and Lennart Bergström. Relating the molecular structure of comb-type superplasticizers to the compression rheology of mgo suspensions. *Cement and Concrete Research*, 36(7):1231–1239, 2006.

[63] Kelly Miller, Renee Melant, and Charles Zukoski. Comparison of the compressive yield response of aggregated suspensions: pressure filtration, centrifugation and osmotic consolidation. *Journal of the American Ceramics Society*, 79(10):2545–2556, 1996.

[64] Chiara Ferraris, Karthik Olba, and Russell Hill. The influence of mineral admixtures on the rheology of cement paste and concrete. *Cement and Concrete Research*, 31(2):245–255, 2001.

[65] F Lange, H Mortel, and V Rudert. Dense packing of cement pastes and resulting consequences on mortar properties. *Cement and Concrete Research*, 27(10):1481–1488, 1997.

[66] V Ramachandran. *Concrete Admixtures Handbook, Properties, Science and Technology*. Noyes Publications, Park Ridge, NJ, 1995.

[67] Gengying Li and Xiaozhong Wu. Influence of fly ash and its mean particle size on certain engineering properties of cement composite moratrs. *Cement and Concrete Research*, 35(6):1128–1134, 2005.

[68] Sun Wei, Yan Handong, and Zhan Binggen. Analysis of mechanisms on water-reducing effect of fine ground slag, high-calcium fly ash and low-calcium fly ash. *Cement and Concrete Research*, 33(8):1119–1125, 2003.

[69] Dale Bentz, Ole Jensen, Kurt Hansen, John Olesen, Henrik Stang, and Claus-Jochen Haecker. Influence of cement particle-size distribution on early age autogenous strains and stresses in cement-based materials. *Journal of the American Ceramic Society*, 84(1):129–135, 2001.

[70] Nathan Tregger, Margaret Pakula, and Surendra Shah. Influence of micro- and nano clays on the fresh state of concrete. *Transportation Research Record: Journal of the Transportation Research Board*, 2141:68–74, 2010.

[71] Bekir Pekmezci, Thomas Voigt, Kejin Wang, and Surendra Shah. Low compaction energy concrete for improved slipform casting of concrete pavements. *ACI Materials Journal*, 104(3):251–258, 2007.

[72] François de Larrard. *Concrete mixture proportioning: A scientific approach*, volume 9 of *Modern Concrete Technology*. E & FN Spon, New York, NY, 1999.

[73] Thierry Sedran and François de Larrard. Optimization of self compacting concrete thanks to packing model. In Åke Skarendahl and Örjan Petersson, editors, 1^{st} *International RILEM Symposium on Self-Compacting Concrete*, pages 321–332, Stockholm, Sweden, September 13-14 1999. RILEM, RILEM Publications S.A.R.L.

[74] M Cintré. Recherche dun mode opératoire de mesure de compacité de mélanges vibrés à sec de classes élémentaires de granulats. Technical report, Les Laboratoires Régionaux des Ponts et Chaussées de Blois, 1988.

[75] V Kantha and S Krishamoothy. Aggregate mixtures for least-void content for use in polymer concrete. *Cement, Concrete and Aggregates*, 15(2):97–107, 1993.

[76] A Joisel. Composition des bétons hydrauliques. *Annales de lITBTP*, 5(58), 1952.

[77] François de Larrard, Thierry Sedran, and D. Angot. Prévision de la compacité des mélanges granulaires par le modèle de suspension solide. II: Validations et cas des mélanges confinés. *Bulletin de Liaison des Laboratoires des Ponts et Chaussées*, 194:71–86, 1994.

[78] Mark Schultz and Leslie Struble. Use of oscillatory shear to study flow behavior of fresh cement paste. *Cement and Concrete Research*, 23(2):273–282, 1993.

[79] L Nachbaur, J Mutin, André Nonat, and L Choplin. Dynamic mode rheology of cement and tricalcium silicate pastes from mixing to setting. *Cement and Concrete Research*, 31(2):183–192, 2001.

[80] Zhihui Sun, Thomas Voigt, and Surendra Shah. Rheometric and ultrasonic investigations of viscoelastic properties of fresh portland cement pastes. *Cement and Concrete Research*, 36(2):278–287, 2006.

[81] Andréa Betioli, Philippe Gleize, Denise Silva, Vanderley John, and Rafael Pileggi. Effect of hmec on the consolidation of cement pastes: isothermal calorimetry versus oscillatory rheometry. *Cement and Concrete Research*, 39(5):440–445, 2009.

[82] Jae Hong Kim, Surendra Shah, Zhihui Sun, and Hyo-Gyoung Kwak. Ultrasonic wave reflection and resonant frequency measurements for monitoring early-age concrete. *Journal of Materials in Civil Engineering*, 21(9):476–483, 2009.